Hmedat *et al.*
Cell Communication and Signaling (2025) 23:293
https://doi.org/10.1186/s12964-025-02129-8

Cell Communication and Signaling

RESEARCH

Open Access

The Src family kinase inhibitor drug Dasatinib and glucocorticoids display synergistic activity against tongue squamous cell carcinoma and reduce MET kinase activity

Ali N. A. Hmedat[1,2], Jessica Doondeea[3], Daniel Ebner[4], Stephan M. Feller[1] and Marc Lewitzky[1*]

Abstract

Background Tongue squamous cell carcinoma (TSCC) is an aggressive cancer associated with a poor prognosis and limited treatment options, necessitating new drug targets to improve therapeutic outcomes. Our current work studies protein tyrosine kinases as well-known targets for successful cancer therapies. It focuses on Src family kinases (SFK), which are known to play a critical role in some head and neck tumors.

Methods Western blot analyses of phospho-tyrosine protein patterns in 34 TSCC lines facilitated the investigation of SFK as contributors to these phosphorylations. The SFK inhibitors PP2 and Dasatinib were utilized to determine SFK contributions to cell motility and survival. A high-throughput screen with 1600 FDA-approved drugs was performed with three TSCC lines to discover drugs that act synergistically with Dasatinib against TSCC cell viability. Glucocorticoids emerged as potential candidates and were further investigated in 2D culture and by 3D soft agar colony formation. Dexamethasone was chosen as the major tool for our analyses of synergistic effects of Dasatinib and glucocorticoids on TSCC lines. Effects on the cell cycle were investigated by flow cytometry and expression levels of cell cycle regulators. Senescence was analyzed by senescence-associated β galactosidase detection and p27Kip1 protein expression. Autophagy was measured by Acridine Orange staining.

Results A panel of 34 TSCC lines showed a surprisingly homogenous pTyr-protein pattern and a prominent 130 kDa pTyr-protein. Inhibition of SFK activity greatly reduced overall pTyr-protein levels and p130Cas tyrosine phosphorylation. It also impaired TSCC viability in 2D cell culture and 3D soft agar colony formation. A high-throughput drug combination screen with Dasatinib identified glucocorticoids as promising candidates for synergistic activity. Dasatinib and Dexamethasone combination treatment showed strong synergistic effects on Src and p130Cas phosphorylation and led to reduced p130Cas expression. Dexamethasone also suppressed phosphorylation of the MET kinase and its key substrate Gab1. On the cellular level, Dasatinib combination with glucocorticoids led to G1 cell cycle arrest, appeared to increase senescence and enhanced autophagy. This was also reflected by effects on cell cycle regulatory proteins, including CDKs and cyclins.

Conclusion This work is the first to show a strong synergistic activity of Dasatinib in combination with clinically used glucocorticoids in solid tumors. Furthermore, the tyrosine kinase MET and its effector protein Gab1 are newly

*Correspondence:
Marc Lewitzky
marc.lewitzky@uk-halle.de
Full list of author information is available at the end of the article

identified glucocorticoid targets. Given the extensive research on MET as a drug target in various cancers, our findings have the potential to advance future cancer treatments.

Keywords Tongue squamous cell carcinoma, Combination therapy, Targeted therapy, Glucocorticoids, Src family kinases

Introduction

Tongue squamous cell carcinoma (TSCC) is a serious public health problem with significant morbidity and mortality [1]. Surgery, in combination with radiotherapy, is often the primary treatment option [2]. Total glossectomy, associated with a high level of morbidity, is performed for advanced carcinomas [3, 4]. With these limited options, more effective treatment options are urgently needed.

Previous analyses, which investigated the mutational features of head and neck squamous cell carcinomas (HNSCC), including different TSCC, revealed various mutations in genes of therapeutic and prognostic significance [5, 6]. In these studies, apart from the mutations in the prominent tumor suppressor gene p53, affected pathways include EGF family receptor signaling, the mitogen-activated protein kinase (MAPK) and NOTCH signaling pathways, as well as adherens junction and focal adhesion pathways. However, many other mutations and dysfunctional regulatory mechanisms likely remain to be discovered.

Molecularly targeted therapies currently play a limited role in head and neck cancers (HNCs). Treatment with the monoclonal anti-EGFR antibody Cetuximab has shown some clinical benefits. However, although there are now numerous additional targeted therapies for patients with HNC in clinical testing [7], there is no particularly effective molecularly targeted therapy for TSCC available until now. Due to the high risk of recurrence and the poor prognosis in TSCC, the search for effective clinical treatments remains an important topic. Identification of new molecular targets may enable significantly improved treatments.

Protein tyrosine kinases (PTKs) play key roles in cellular signal transduction, cell cycle regulation, cell division, and cell differentiation. The signaling pathways regulated by protein kinases are frequent targets of mutations, leading to many human cancers [8]. Dysregulation of PTK-activated pathways, often by overexpression, gene amplifications, or genetic mutations, are causal factors underlying numerous cancer developments, as well as disease progression and drug resistance [9]. The inhibitions of kinases with drugs have produced substantial antitumor effects for some cancer types.

To detect tyrosine kinases which might become therapeutic targets in TSCC treatment we have studied tyrosine phosphorylation in a panel of 34 TSCC lines. Western blot analysis of their protein tyrosine phosphorylation status, using a well-established anti-phosphotyrosine antibody, revealed a surprisingly homogenous pTyr-protein pattern throughout the TSCC panel with a prominent 130 kDa pTyr-protein. This led us to focus initially on the potential involvement of the multi-site docking protein p130Cas (BCAR1) and Src family kinases (SFK), which are readily known to play important roles in some head and neck cancers [10]. Inhibition of SFK activity with two inhibitors, the tool compound PP2 [11] and the clinically used drug Dasatinib (DAS) [12], greatly reduced overall pTyr-protein levels and p130Cas tyrosine phosphorylation on specific epitopes. Moreover, TSCC viability in standard cell culture and 3D soft agar colony formation was greatly diminished.

Since monotherapies with anti-cancer drugs are frequently ineffective or short lasting in their activity and thus require additional drugs to accomplish useful clinical responses [13–15], we performed a high-throughput screen with 1600 FDA-approved drugs, to discover candidate molecules that achieve synergistic activity against TSCC lines when combined with DAS. This screen identified glucocorticoids (GCs), including Dexamethasone and Fluticasone, as a promising group of drugs for further analyses. GCs have been widely used in medicine for decades, including as part of some cancer treatment regimens [16, 17]. The expansion of their clinical use in cancer therapies could be swift and cost-effective, with only moderate concerns about off-target toxicities. After more detailed studies, GCs were found to induce rapid and prolonged inhibition of the MET tyrosine kinase. This suggests that GCs may have a useful role to play in the clinical inhibition of MET signaling in tumors. MET has a range of substrate proteins. However, for this study, we decided to focus on its key substrate Gab1, a ubiquitous multi-site docking protein, which shows, when eliminated by targeted disruption in mice, a phenotype very similar to a MET knockout [18, 19]. Effects elicited on MET were echoed in the Gab1 phosphorylation patterns, suggestive of a functional role for Gab1 in at least some of the pleiotropic effects of GCs.

Results

Similarity of tyrosine phosphorylation patterns and prominence of a 130 kDa pTyr-protein in a panel of 34 TSCC lines

Tyrosine kinases are frequent drivers of human tumor development but remain only marginally studied in TSCC. Identifying tyrosine kinases that are overexpressed or hyperactivated in TSCC should enable us to think more rationally about targets to counteract this devastating disease. To gain a first insight into the abundance and sizes of pTyr-proteins in TSCC, total cell lysates from 34 cell lines (30 established from primary tumors, 4 from metastases) were subjected to Western blot analysis of the protein tyrosine phosphorylation status using an anti-phosphotyrosine antibody (Figure S1). Further information on the cell lines can be found in Suppl. Table 1 and in [20].

Cells were fed with an excess of culture medium 48 h before harvesting, to minimize medium effects on pTyr-protein and to obtain information on the cells' 'steady state' phosphorylation. Unexpectedly, all TSCCs exhibit fairly similar tyrosine phosphorylation patterns with particularly notable bands at around 130 kDa, possibly indicative of a prominent role of a single kinase or kinase family in TSCC. This is in stark contrast to the diverse pTyr patterns seen in other cancer cell line panels, for example a panel derived from colorectal carcinomas, which display a much greater variability concerning pTyr-protein abundances and band patterns [21]. p130Cas is a well-known and major substrate protein of several oncogenic tyrosine kinases, including Src and Abl family kinases [22–24] and was therefore analyzed in the TSCC panel.

Identification of p130Cas (BCAR1) as ubiquitous pTyr-protein in the TSCC line panel

p130Cas contains numerous potential tyrosine phosphorylation sites that are mostly clustered in the 'substrate region' of the protein. p130Cas (later also named BCAR1) has been characterized as a docking and signal processing platform for multiple signal transduction proteins [25–27]. To check for the total protein levels and phosphorylation status of p130Cas, total cell lysates from the 34 TSCC lines were analyzed by Western blotting (Figs. 1A and S1).

The p130Cas protein is expressed throughout all cells of the cell line panel. It had been shown previously to travel as multiple bands in gel electrophoresis [22, 28]. The protein is also phosphorylated in all TSCC lines on Tyr 410 (Y410), a major phosphorylation site and binding motif for Crk family adaptor proteins [29]. However, since p130Cas is well known to be phosphorylatable on more than a dozen tyrosines (see *phosphosite.org* and references therein), this phospho-antibody, raised against a single phosphorylation site of p130Cas, does not necessarily reflect the overall phosphorylation detected by the pTyr-antibody. From these initial results, we surmised that p130Cas is probably a major component of the 130 kDa phospho-tyrosine band detected in all TSCC lines of the panel and that it might be a potential therapeutic target for tongue cancer. However, the non-catalytic nature of p130Cas makes it difficult to develop specific inhibitors. Therefore, alternative strategies are needed to inhibit p130Cas activity.

Src family kinases are essential for maintaining the tyrosine phosphorylation of p130Cas and other pTyr-proteins in TSCC lines

Previous work has shown that the C-terminal region of p130Cas contains a Src kinase binding domain and that the association between p130Cas and activated Src kinase is essential for the tyrosine phosphorylation and activation of p130Cas by Src at least in some cells [30]. Therefore, SFK inhibitors have been proposed as useful tools to inhibit p130Cas activity. Hence, the effect of the SFK inhibitor compound PP2 [31–33] on the overall pTyr-protein levels and p130Cas activity was analyzed in SAS cells (Figure S2A). SAS cells were chosen for these initial experiments since they are widely studied, fast growing and highly motile, presumably representing a particularly aggressive form of TSCC.

Upon PP2 treatment of SAS cells, a substantial drop in tyrosine phosphorylation was observed at all time points. A control compound, PP3, which lacks SFK blocking activity, did not lead to detectable pTyr pattern changes. p130Cas pY410 phosphorylation was also clearly reduced after PP2 application. During these experiments, striking effects on SAS cell survival and proliferation were noticed, which led us to investigate the crucial proliferation-regulating MAP kinases Erk1 and Erk2 as well. Severe reductions in the levels of active Erk1/2 were apparent. Blotting with a Src pY416 antibody, expectedly, also showed a rapid decline in the activity-regulating tyrosine phosphorylation of SFK. This tyrosine residue is well-known to contribute to the regulation of Src activity [34] and the Tyr416 phospho-antibody recognizes several SFK members that share a high degree of homology in their relevant protein epitopes [21].

Live cell imaging of SAS cells reveals pleiotropic effects of tyrosine kinase inhibition with PP2

SAS cells treated with PP2 show a striking growth inhibition compared to DMSO-treated control cells. To analyze this further, live cell imaging was performed. Detailed inspection of the videos of SAS cells treated with DMSO or PP2 further documented that PP2 can exert several

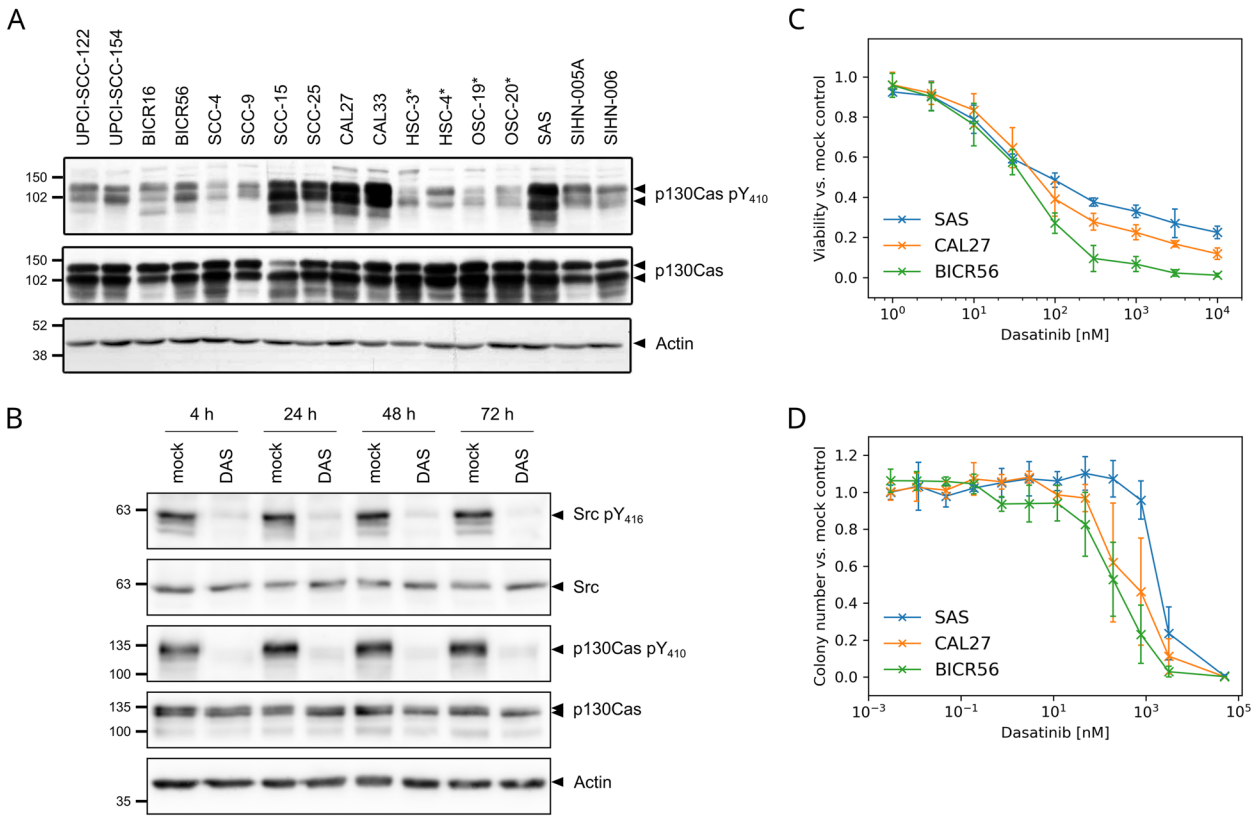

Fig. 1 Dasatinib reduces the growth of TSCC cells and causes inhibition of Src pTyr416 and p130Cas pTyr410 phosphorylation. **A** Total TSCC cell lysates were separated by SDS-PAGE and analyzed by Western blotting with the indicated antibodies. Actin serves as loading control. Cell lines derived from metastases are marked by asterisks. **B** Western blot analysis of the total level and the phosphorylation level of Src and p130Cas in SAS cells treated with DMSO as vehicle control (mock) or 100 nM of Dasatinib (DAS) for the indicated time points. **C** Dose–response curves for DAS in TSCC lines as determined by resazurin assay after 72 h treatments. Values are normalized to mock-treated cells. The dose–response curves show mean values ± SD for three independent experiments with six parallel measurements each. **D** Dose–response curves of TSCC lines treated with DAS as determined by colony formation in 3D soft agar assay. Cells were treated with DMSO as vehicle control (mock) or different concentrations of DAS. Colony numbers were normalized to mock-treated cells. The dose–response curves show mean values ± SD of three independent experiments with at least 2 wells counted in each case

biological effects (Video S1). Not only does PP2 inhibit the swarm-like cell migration of SAS cells and their cell proliferation, but it also induces a substantial change in cell morphology, and, possibly, a reversion of epithelial-mesenchymal transition (EMT) [33]. Before PP2 application, individual cell boundaries are clearly visible. These disappear upon cell exposure to PP2, but not DMSO alone, yielding more dense epithelial sheets. Starting after approximately 24 h of treatment and more prominently visible from ca. 40 h onward, membrane blebbing and cell death is also observed. All of these effects of tyrosine kinase inhibition would be expected to be anti-oncogenic.

Dasatinib reduces TSCC lines growth in a dose-dependent manner and inhibits Src family kinase activity

Since PP2 is just a tool compound and not approved for cancer treatments, we decided to further investigate the SFK inhibition effect on the reduction of p130Cas activity and the growth of TSCC using the clinically important SFK inhibitor Dasatinib (DAS) [35]. DAS is approved, for example, for the treatment of chronic myelogenous leukemia (CML) refractory to or intolerant of Imatinib, but also as first-line treatment of chronic-phase CML and for patients with Philadelphia chromosome-positive acute lymphoblastic leukemias [35].

Initially, SAS cells were treated with 100 nM DAS, a clinically achievable concentration [36], for increasing durations (from 4 h up to 72 h). DAS caused an almost complete inhibition of SFK and p130Cas phosphorylations, as determined by western blots with anti-pY416 Src and anti-pY410 p130Cas, respectively (Fig. 1B). This inhibition was apparent at all time points.

It should be noted that DAS inhibits not only Src but also Abl family kinases, which could contribute to the suppression of overall pTyr levels in the TSCC lines.

The reduced p130Cas phosphorylation may also be the result of Abl inhibition since p130Cas is also well-known Abl substrate [37, 38]. To determine if SFK inhibition accounts for the observed reduction of overall pTyr levels and p130 Cas pY410, we also tested the clinically used Abl family kinase inhibitor Imatinib on SAS cells. In addition to Abl family kinases, Imatinib can also inhibit c-Kit, PDGFR and other kinases, but it has no prominent effect on SFKs [39]. DAS, but not Imatinib, reduced pTyr, p130Cas pY410 and SFK pY416 levels in a dose-dependent manner (Figure S2B). These data indicate that SFK inhibition by DAS and not Abl inhibition is very likely responsible for massively decreasing pTyr-protein levels in TSCC.

Subsequently, three TSCC lines (SAS, CAL27 and BICR56) were selected from the large TSCC panel to represent different patterns and levels of tyrosine phosphorylation (Figure S1). The cell lines also represent different mutational backgrounds [40], are easily available and are suitable for xenografts [41–43]. These cell lines were treated with different concentrations of DAS for 72 h. Cell viability under standard cell culture (2D) conditions was then determined by resazurin assay. As shown in Fig. 1C, cell viability was reduced in a dose-dependent manner in all three cell lines. These results indicate that DAS has clear activity against TSCC cells in 2D culture. The SAS cell line shows a lesser response to DAS compared to the other 2 cell lines, with BICR56 being the most sensitive cell line. DAS did not eliminate all SAS and CAL27 cells, even at very high concentrations (10 μM) after 72 h of exposure, which suggests that the effects of DAS on cell growth are, at least in part, antiproliferative/cytostatic and not entirely cytotoxic.

To investigate the effects of DAS on TSCC cell lines in 3D culture, a classical soft agar assay, which can, to some degree, mimic the growth of cancer cells in actual tissues, was employed. TSCC cells were seeded into soft agar layers and treated with different concentrations of DAS. Cells were maintained in culture for 14 days to allow the formation of colonies. DAS greatly reduces colony formation SAS, CAL27 and BICR56 in a dose-dependent manner, as shown in Figs. 1D and S4C.

A high-throughput drug combination screen identifies drugs acting synergistically with Dasatinib on TSCC lines

Small, early phase clinical trials with exploratory SFK inhibitor treatments of unselected head and neck cancer patients have so far failed to show significant clinical benefits [13–15]. The underlying reasons for this lack of clinical activity as monotherapies remain to be identified. However, nearly all effective cancer treatments are currently based on the additive or even synergistic actions of several drugs applied in combination [44, 45].

To identify drug candidates that display synergistic activity together with DAS from the large collection of existing FDA-approved drugs, we performed high-throughput screens using the Pharmakon 1600 library on SAS, CAL27 and BICR56 cells. Details of the screens are described in Materials and Methods. Briefly, drugs that showed an outstanding ratio of cell metabolic activity impairment in combination with DAS compared to cell metabolic activity impairment for the drug alone, in more than one cell line, were considered for further analyses (Supplementary Data S1). For the SAS cell line, a majority of candidate drugs were effectors of glucocorticoid or β-adrenergic signaling stress receptor signaling pathways. Two drugs, the glucocorticoid Fluticasone and β2-adrenergic receptor agonist Isoproterenol were also found to have synergistic activity on the BICR56 cell line. Initial experiments with β2-adrenergic receptor agonists were not successful and so it was decided to focus on the potential synergy of DAS and glucocorticoids for further work.

To assess the possible synergistic activity between DAS and Fluticasone (FL), SAS cells were initially treated with increasing concentrations of FL as single agents, or with a fixed concentration of FL in combination with increasing concentrations of DAS. Cell viability was examined by resazurin assay after 72 h of treatment. FL alone has no significant effect on SAS cell viability up to a concentration of 10 μM (Figure S3A). Next, clinically relevant concentrations up to 100 nM of FL [46] were tested in combination with DAS. 25 nM of FL was sufficient to significantly enhance the cell toxicity of DAS in the SAS cells (Figure S3B).

To confirm the cytotoxic effect of the DAS + FL against TSCC, trypan blue dye exclusion assays were performed. 50 nM of DAS was combined with 25 nM of FL. After 72 h treatments, cells were trypsinized, mixed with dye and the numbers of viable cells were counted with an automated cell counter and normalized to mock-treated cells (Figure S3C). The proliferation of all TSCC lines tested was strongly reduced in the presence of DAS + FL versus DAS alone. Again, individual application of FL showed no significant effect. The trypan blue assay results thus confirm the synergistic activity of the DAS + FL combination treatment found in the resazurin assay.

While these results were certainly encouraging, it should be noted, that FL suffers from low oral bioavailability and its clinical utilization is limited to topical routes of administration [47]. Therefore, it was decided to investigate systemically applicable GCs, to determine whether they also show synergistic effects in TSCC lines in combination with DAS.

Dasatinib + Dexamethasone combination treatment shows a strong synergistic effect against TSCC cells in 2D and 3D cultures

Dexamethasone (DX) is a long-acting GC, available in multiple dosage forms, which is used to treat a large variety of diseases [48]. It therefore seemed to be a highly suitable candidate in search for synergistic GC—DAS activities. SAS cells were thus treated with DX or DAS as single agent or with DAS + DX combinations and the cell viability was measured by resazurin assay after 72 h. DX treatment alone showed no substantial effect on the metabolic activity of SAS cells at concentrations of up to 10 μM (Fig. 2A). 100 nM of DX sensitized SAS cells to DAS and synergistically enhanced its effect on cell viability (Fig. 2B). All investigated TSCC lines showed clear responses, with the effect being more pronounced for the SAS cell line than for CAL27 and BICR56 (Figures S4A and S4B). To further examine this synergistic interaction in 2D culture, trypan blue dye exclusion assays were conducted to determine the number of viable cells after each treatment. 50 nM of DAS was combined with 100 nM of DX. After 72 h, viable cells were counted and normalized to mock-treated cells. A combination of DX and DAS reduced the number of viable cells drastically and more strongly than DAS alone (Fig. 2E).

Subsequently, soft agar colony formation assays were performed to investigate the effects of DAS + DX treatment on anchorage independent growth. As shown in Fig. 2C, DX by itself did not cause any substantial colony formation reduction in SAS cells, even at a very high dose of 10 μM. In contrast, DAS on its own reduced colony formation in a dose-dependent manner (Fig. 2D, Figure S4C). This was also observed in Cal27 and BICR56 cells (Figures S4D and S4E). The dose–response curves for the combination treatments show that 100 nM of DX and DAS synergistically reduce colony formation in TSCC lines. SAS cells, which showed the weakest response to DAS treatment alone, with an IC_{50} value of around 2000 nM, displayed high sensitivity to the combination treatment. The IC_{50} value was reduced by a factor of 58 when adding 100 nM DX (Fig. 2F). CAL27 cells displayed an even greater responsiveness to the DAS + DX treatment. The IC_{50} decreased by a factor of 145 from around 500 nM with DAS alone to 3.2 nM with DX + DAS. DAS + DX treatment showed less synergistic activity in BICR56 cells, but the IC_{50} was still reduced 11 times by the combination treatment.

Dasatinib + Dexamethasone combination treatment leads to a pronounced reduction of p130Cas expression

Next, we investigated the molecular effects of DAS in combination with DX on Src and p130Cas. TSCC lines were treated with DMSO (mock), 50 nM of DAS, 100 nM of DX or 50 nM DAS plus 100 nM DX for 72 h, followed by Western blot analyses. As before, DAS alone strongly inhibited Src and p130Cas phosphorylation. This was not enhanced by addition of DX (Fig. 3). However, DAS + DX reduced the total levels of p130Cas (Figure S9A). The same was also observed for DAS + FL treatment (data not shown). This suggests that the biological effects seen with DX could, at least to some degree, result from effects on the p130Cas protein. However, GCs are well-known to induce rather pleiotropic effects on cell signaling in different cell contexts [49], so various other signaling pathways have to be considered.

Dexamethasone treatment suppresses MET kinase signaling in TSCC lines

Src has been shown to interact with a range of receptor tyrosine kinases (RTKs), either as a downstream target, or even as an upstream effector, as we have previously shown for the RTK mesenchymal-epithelial transition factor (MET) in colorectal cancer cell lines [21]. Overexpression of MET has been observed in more than 80% of head and neck squamous cell cancers and preclinical and clinical studies have linked MET overexpression to cellular proliferation, invasion, migration, and poor prognosis [50]. Thus, we next analyzed the expression and phosphorylation of MET and its key substrate protein Gab1 upon treatment with DAS and DX, either alone or in combination for 72 h, in the three TSCC lines.

MET phosphorylation at Y1234/1235, Gab1 phosphorylation at Y627 (a docking site for the proliferation-driving phosphatase Shp2) and total protein levels were assessed by Western blotting. As shown in Fig. 4A, MET phosphorylation was somewhat reduced by DAS, but, surprisingly, greatly diminished upon DX treatment. The same pattern was observed for Gab1 pY627. Both drugs showed no major effect on the total MET and Gab protein levels, although the mature form of the MET receptor kinase (upper band [51]) may be somewhat reduced, possibly indicating some effect on proteolytic MET processing.

To determine how fast the DX effects on MET and Gab1 phosphorylation occur, we incubated SAS cells with DX for up to 72 h and collected samples at different time points. As shown in Fig. 4B, MET dephosphorylation became obvious after 4 h, reached a maximum at 24 h and persisted for at least 72 h. This correlated with the repression of phosphorylation at Y627 of the MET downstream target Gab1. The somewhat delayed inhibition of MET phosphorylation suggested to us that DX is probably not a direct inhibitor of MET kinase activity. To test this assumption, a MET kinase activity assay was performed. Briefly, MET was immunoprecipitated from SAS cell lysates and incubated

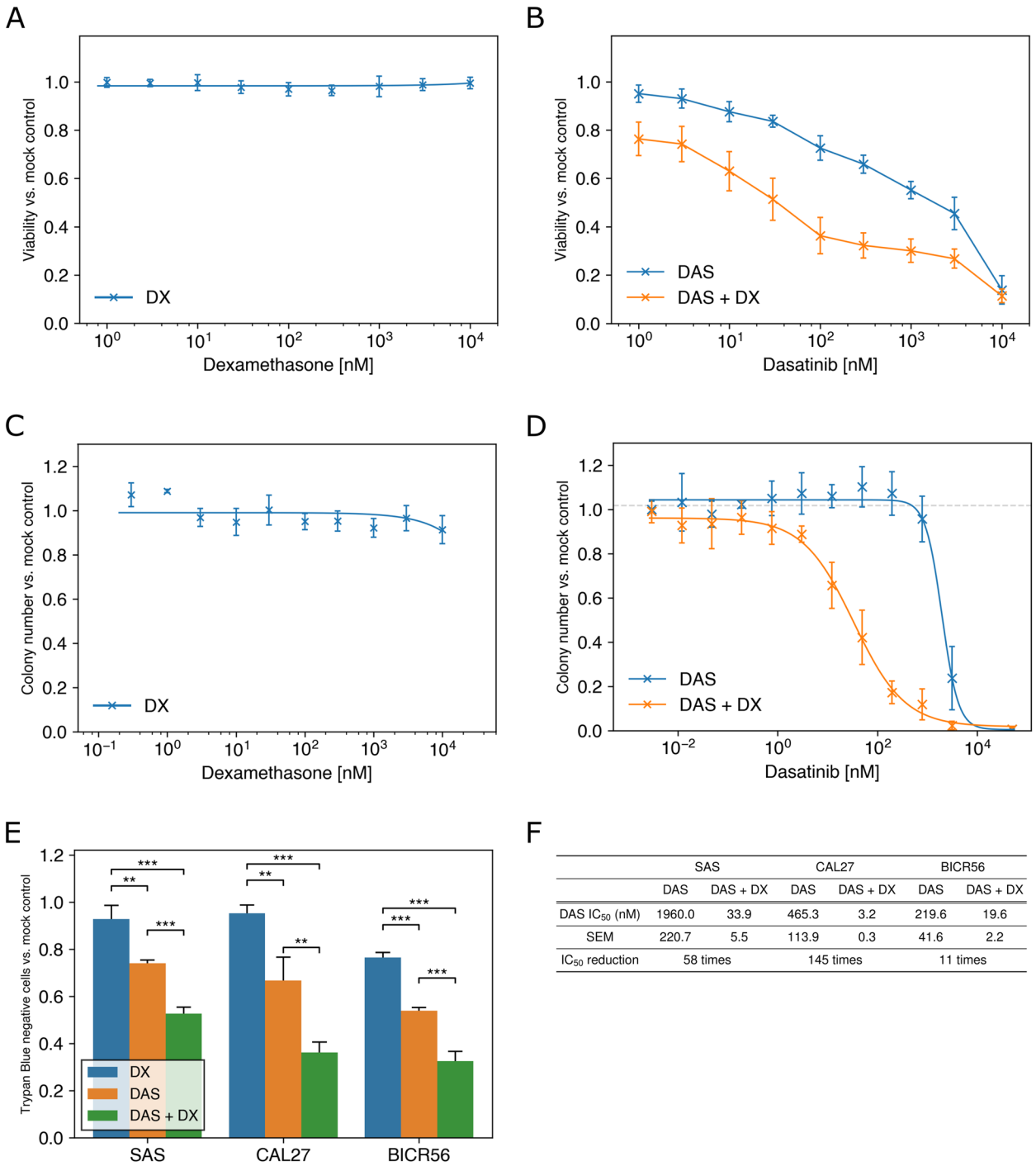

F

	SAS		CAL27		BICR56	
	DAS	DAS + DX	DAS	DAS + DX	DAS	DAS + DX
DAS IC_{50} (nM)	1960.0	33.9	465.3	3.2	219.6	19.6
SEM	220.7	5.5	113.9	0.3	41.6	2.2
IC_{50} reduction	58 times		145 times		11 times	

Fig. 2 Dasatinib + Dexamethasone combination treatment shows a synergistic effect on TSCC cells in 2D and 3D cell cultures. **A** Dose–response curves of SAS cells treated with different concentrations of DX in 2D culture for 72 h as analyzed by resazurin assay. **B** Dose–response curves of SAS cells treated with different concentrations of DAS with or without 100 nM DX for 72 h. Cell viability was measured by resazurin assay. **C** Colony numbers in 3D soft agar culture for SAS cells treated with different concentrations of DX. **D** Dose–response curves of SAS cells treated with DAS with or without 100 nM DX, as determined by colony numbers in 3D soft agar culture. **E** TSCC lines were treated with DMSO as vehicle control (mock), 50 nM of DAS, 100 nM of DX, or DAS + DX for 72 h. Cell numbers were evaluated by staining cells with trypan blue and counting of viable cells with an automated cell counter. Asterisks indicate statistical significance for T-tests with *p*-values at less than 0.05 (*), less than 0.01 (**) or less than 0.001 (***), respectively. In A to E, data were normalized to mock-treated cells and values are expressed as means and standard deviation obtained from three independent experiments. **F** Comparison of the average IC_{50} values for DAS alone and DAS + 100 nM DX in TSCC lines assessed by 3D soft agar culture. IC_{50} values were derived by fitting a four-parameter log-logistic function. Values are presented as the means ± SEM for three independent experiments

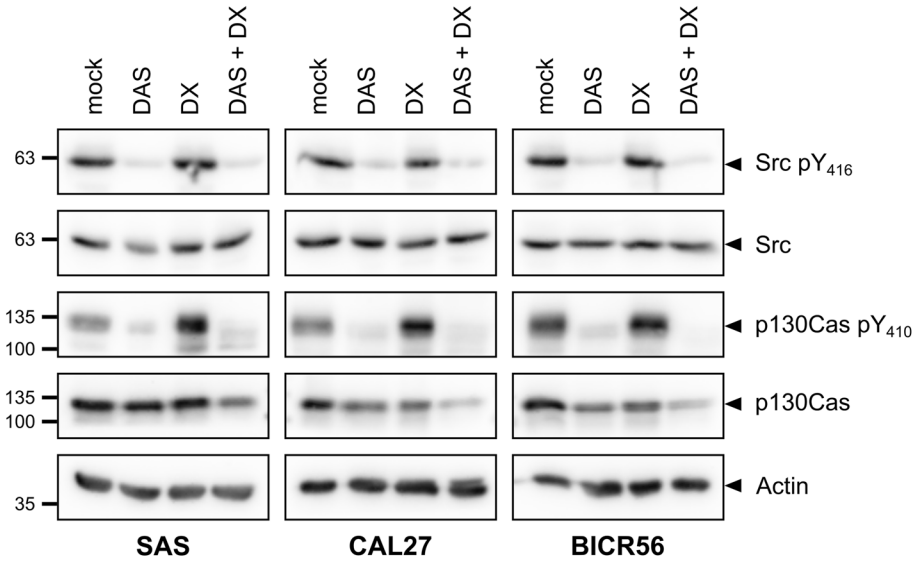

Fig. 3 Dasatinib inhibits phosphorylation of Src and p130Cas, Dasatinib + Dexamethasone co-treatment reduces p130Cas protein levels. Western blot analysis of Src and p130Cas expression, as well as Src and p130Cas phosphorylation, in SAS, CAL27 and BICR56 cells treated with DMSO (mock control), 50 nM DAS, 100 nM DX, or a combination of DAS + DX for 72 h

with ATP plus a recombinantly expressed fragment of Gab1 (aa 613–694) as kinase substrate. DMSO, 100 nM DX, 500 nM DX or 100 nM Crizotinib (a potent and direct MET kinase inhibitor) were added to the kinase reaction. The results, shown in Figure S5, indicate that, unlike Crizotinib, DX is no direct inhibitor of MET kinase activity at a concentration of 500 nM, which is approximately 5 times higher than the pharmacologically achievable plasma concentration.

To define the potency of DX and to investigate, if the inhibitory effect on MET can also be seen with another GC, SAS cells were treated with different concentrations of DX or FL for 72 h in the absence of any DAS. Strikingly, subnanomolar concentrations of either GC were already sufficient to inhibit MET phosphorylation substantially (Fig. 4C). The exact mechanism of the surprising and potent effect of GC on the MET—Gab1 signaling pathway remains to be further investigated. In addition, GCs, as mentioned above, may have significant effects on additional cellular signaling pathways.

Dasatinib + Dexamethasone combination treatment induces G1 cell cycle arrest and may increase senescence in TSCC cells

In a subsequent set of experiments, we aimed to determine the effects of DAS, DX and their combination on the cell cycle and its regulatory proteins. The three TSCC lines were treated with DMSO (mock), 50 nM DAS, 100 nM DX, or a combination of DAS + DX for 72 h and thereafter stained with DAPI for determination of their DNA content by flow cytometry (Fig. 5A). Individually, both compounds induced a slight increase of cells in the G1 phase, while combination treatment caused more significant G1 arrests (SAS: mock 59.7% ± 1.9% vs. DAS + DX 86.2% ± 0.8%, $n = 3$). As expected, cells in S phase were notably reduced (SAS: mock 29.2% ± 0.1% vs. DAS + DX 7.6% ± 0.1%, $n = 3$), as were cells in G2/M phase (SAS: mock 11.1% ± 0.3% vs. DAS + DX 6.2% ± 0.1%, $n = 3$). No significant sub-G1 peak increases, indicative of substantially elevated cell death, were found (data not shown).

(See figure on next page.)

Fig. 4 Dasatinib + Dexamethasone combination treatment suppresses MET kinase signaling. **A** Western blot analysis of MET and Gab1 expression and phosphorylation in TSCC cells treated with DMSO (mock), 50 nM of DAS, 100 nM of DX, or a combination of DAS + DX for 72 h. Antibodies that detect the phosphorylation of MET at Tyr1234/1235 and of Gab1 at Tyr627 were used to monitor changes in phosphorylation levels. **B** Western blot analysis of MET phosphorylation in SAS cells treated with DMSO (mock) or 100 nM of DX for the indicated time points. **C** Western blot analysis of MET phosphorylation in SAS cells treated with the indicated concentrations of FL or DX for 72 h

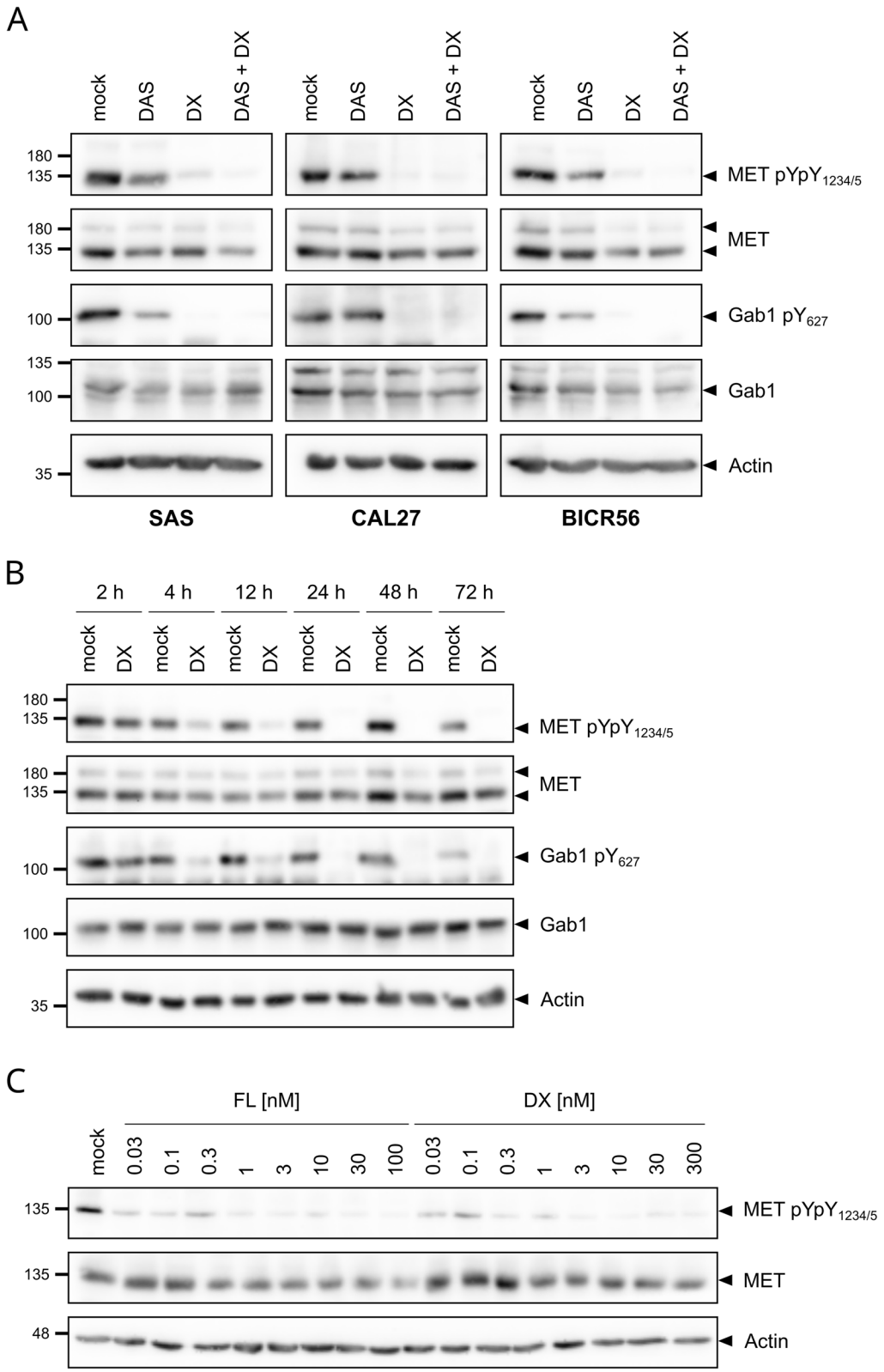

Fig. 4 (See legend on previous page.)

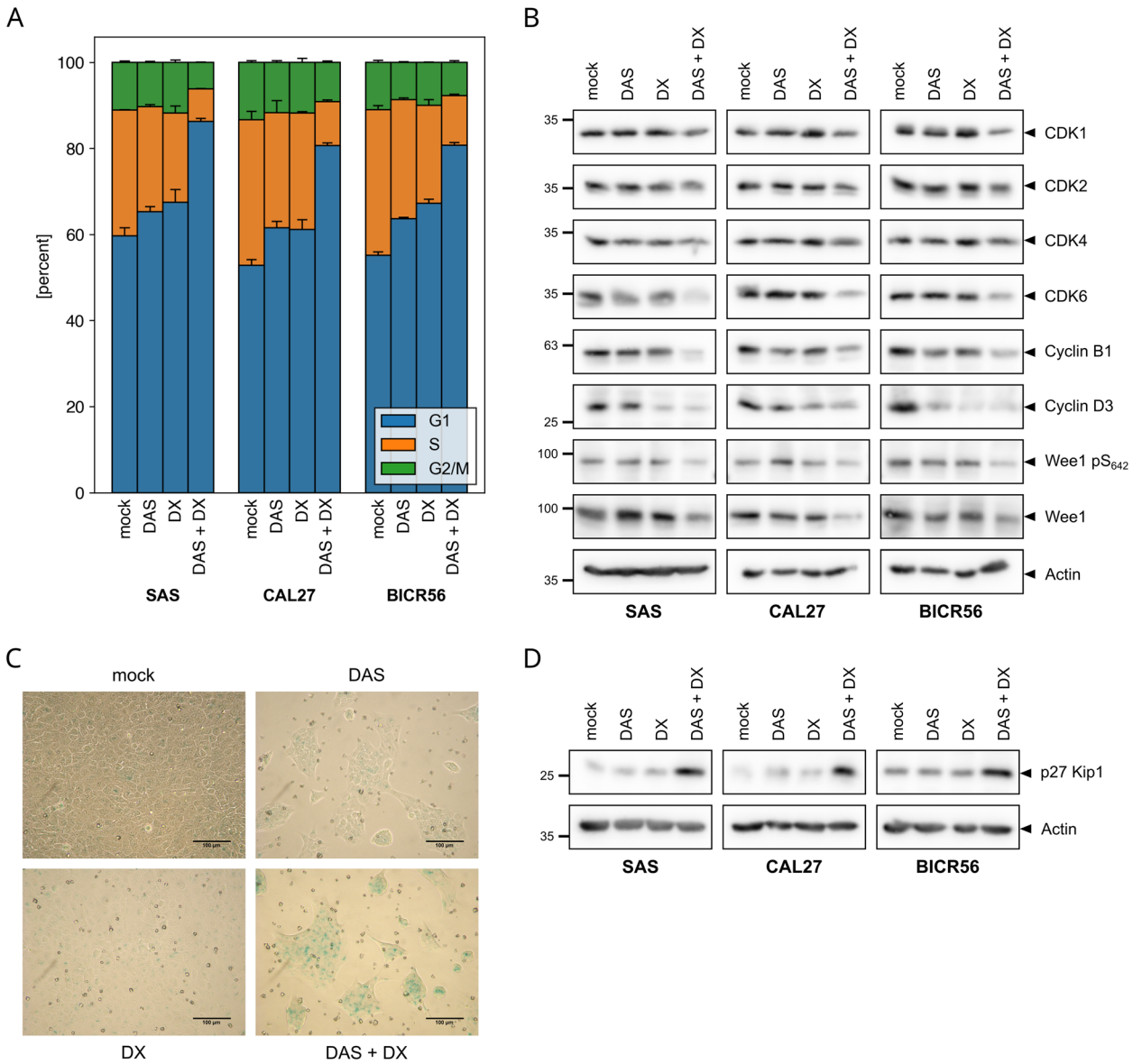

Fig. 5 Dasatinib + Dexamethasone combination treatment induces cell cycle arrest in G1 and senescence. Cells were treated with DMSO (mock), 50 nM of DAS, 100 nM of DX or a combination of DAS + DX for 72 h. **A** Treated TSCC lines were stained with DAPI and DNA contents were determined by flow cytometry. 10,000 cells were analyzed for each experiment. Cell populations are displayed as percentage of cells at each cell cycle phase relative to the total population. Results are expressed as means and standard deviation obtained from 3 independent experiments. **B** Western blot analyses of CDKs, cyclins and Wee1 as indicated. **C** Representative pictures of SAS monolayer cultures stained with senescence-associated-β-Galac tosidase (SA-β-Gal). SA-β Gal positive staining (blue color) indicates aged cells. The scale bar length indicates a length of 100 µm. **D** Western blot analysis of p27Kip1 protein expression

Next, the protein expression levels of several crucial cell cycle regulators were examined in SAS, CAL27 and BICR56 cells using the same treatment conditions (Fig. 5B and Figure S9B). Western blot analyses showed that the levels of the cyclin-dependent kinases CDK1, possibly CDK4 and, especially, CDK6 were reduced upon DX + DAS co-treatment. In addition, we investigated the expression of Cyclin B1, together with CDK1, a gatekeeper for the entry into mitosis, and Cyclin D3 which interacts with CDK4 and CDK6 to regulate G1/S-transition. Both cyclins were reduced by DAS + DX treatment. This agrees with the observed changes in cell cycle phase distributions (Fig. 5A). An additional key player of cell cycle regulation, the Wee1 kinase, an inhibitor of mitosis entry [52], was also examined. The observed total reduction in Wee1, together with dephosphorylation

of pSer642 upon treatment with DAS + DX (Fig. 5B), is expected to reduce nuclear Wee1 and increase its cytoplasmic localization [53]. The changes in CDKs, Cyclins and Wee1 levels, observed so far, warrant a more extended and detailed future investigation of cell cycle regulator signaling in order to determine the functionally relevant alterations elicited by DAS + DX combination treatment.

Besides cell cycle changes, glucocorticoids have also been reported to affect other cell fates, including cellular senescence [54, 55]. These effects can vary, depending on cell type, length of exposure and physiological context [56–58]. Therefore, the consequences of DAS + DX treatment in relation to cellular senescence are hard to predict. To gain a first insight into this, senescence-associated beta-galactosidase (SA-β-gal) assays were performed as described in the methods section. SA-β-gal positive blue staining, which indicates senescent cells, was detected by light microscopy (Fig. 5C and S6A + B). Co-application of DAS and DX for 72 h increased the blue staining. These findings are very preliminary and further studies with a quantification of stained cells would be required. In the following, the expression levels of p27Kip1 were evaluated. p27Kip1 has been reported as a driver for DX-induced senescence and is also a more general inducer of cell cycle blockades due to its interactions with CDK/Cyclin complexes in various normal and cancer cells [56, 59] (Fig. 5D and Figure S9C). Not unexpectedly, p27Kip1 was upregulated in all three TSCC lines after co-treatment with DAS + DX.

Dasatinib + Dexamethasone treatment induces autophagy in TSCC cells

Another biological response altered in cancer cells by some drugs is autophagy, the degradation of cellular material by lysosomes [60]. GCs have been shown to induce autophagy in lymphoid leukemia [61] and pancreatic ductal adenocarcinoma cells [62]. Autophagy has context-dependent roles in cancer. It is thought that autophagy can prevent the development of some cancers, but, once established, it may help cancer cells to survive under supply stress conditions [63–65].

To examine if DAS alone, DX alone, or the combination of DAS plus DX impact on autophagy in SAS, CAL27 and BICR56 cells, accumulation of acidic components and increased volume of acidic vesicular organelles was assessed by Acridin Orange (AO) staining. AO is a fluorophore that accumulates as protonated form in acidic vesicular organelles such as autolysosomes and is commonly used to study late-stage autophagy by fluorescence microscopy or flow cytometry [66]. As shown in Figure S7A, DX treatment alone caused only a small increase in AO fluorescence in SAS cells. DAS alone more than triples the percentage of autophagic cells. DAS + DX co-treatment further increased the proportion of cells with high fluorescence. Repeated measurements ($n = 3$) for all TSCC lines showed a similar response in all TSCC lines (Figure S7B). Upon DAS + DX co-treatment, an especially striking effect was seen for CAL27 cells, again pointing to pleiotropic effects of GCs when combined with DAS.

The glucocorticoids hydrocortisone and methylprednisolone synergize with dasatinib to suppress growth

Since many different glucocorticoids are in clinical use, we also wanted to explore whether other commonly prescribed drugs like Hydrocortisone (HC) and Methylprednisolone (MP) display DX-like activity in TSCC cells**.** For this, SAS cells were treated with DMSO (mock), 50 nM DAS, 300 nM HC or 150 nM MP, as well as combinations of DAS + HC or DAS + MP for 72 h.

As Fig. 6A shows, the cell density of SAS cells in 2D culture is clearly reduced after DAS treatment. This reduction is more pronounced after DAS + HC and DAS + MP combination treatments. To quantify cell numbers, cells were stained with trypan blue and counted. The cell number was reduced upon DAS treatment to ca. 65% of DMSO-treated cells. HC and MP treatment alone reduced viable SAS cells to approximately 80%. The antiproliferative activity of DAS was further increased after addition of HC or MP. The number of viable cells was reduced further from 65 to 48% following DAS + HC or to 42% following DAS + MP combination treatment (Fig. 6B). In follow-up experiments, 3D soft agar colony formation was employed to examine the effects of HC or MP in a slightly more physiological context. Initially, SAS cells were treated with serial dilutions of HC or MP (Fig. 6C + D). Data for CAL27 cells can be found in Supplementary Figure S8A + B. Colonies were counted after 14 days. As already seen for DX (Fig. 2C), no noticeable decrease in colony formation was found for up to 10 µM with either of the GCs (Fig. 6C for SAS and Figure S8A for CAL27). Increasing concentrations of HC or MP were then combined with a marginally active concentration of 1 µM DAS for SAS cells (deduced from Fig. 2D) or 100 nM for CAL27 cells (deduced from Figure S4D). DAS + HC and DAS + MP combination treatments exhibit strong colony formation reduction in a dose-dependent manner (Fig. 6Dand S8B). For HC, which is less potent than MP, a concentration of at least 300 nM was needed to show a notable effect in combination with DAS. MP displays a synergistic activity together with DAS at a concentration comparable to DX (100 nM). This indicates that at least four different GC show similar effects on TSCC growth in 2D and 3D culture. It should be noted that the investigated concentrations of HC and

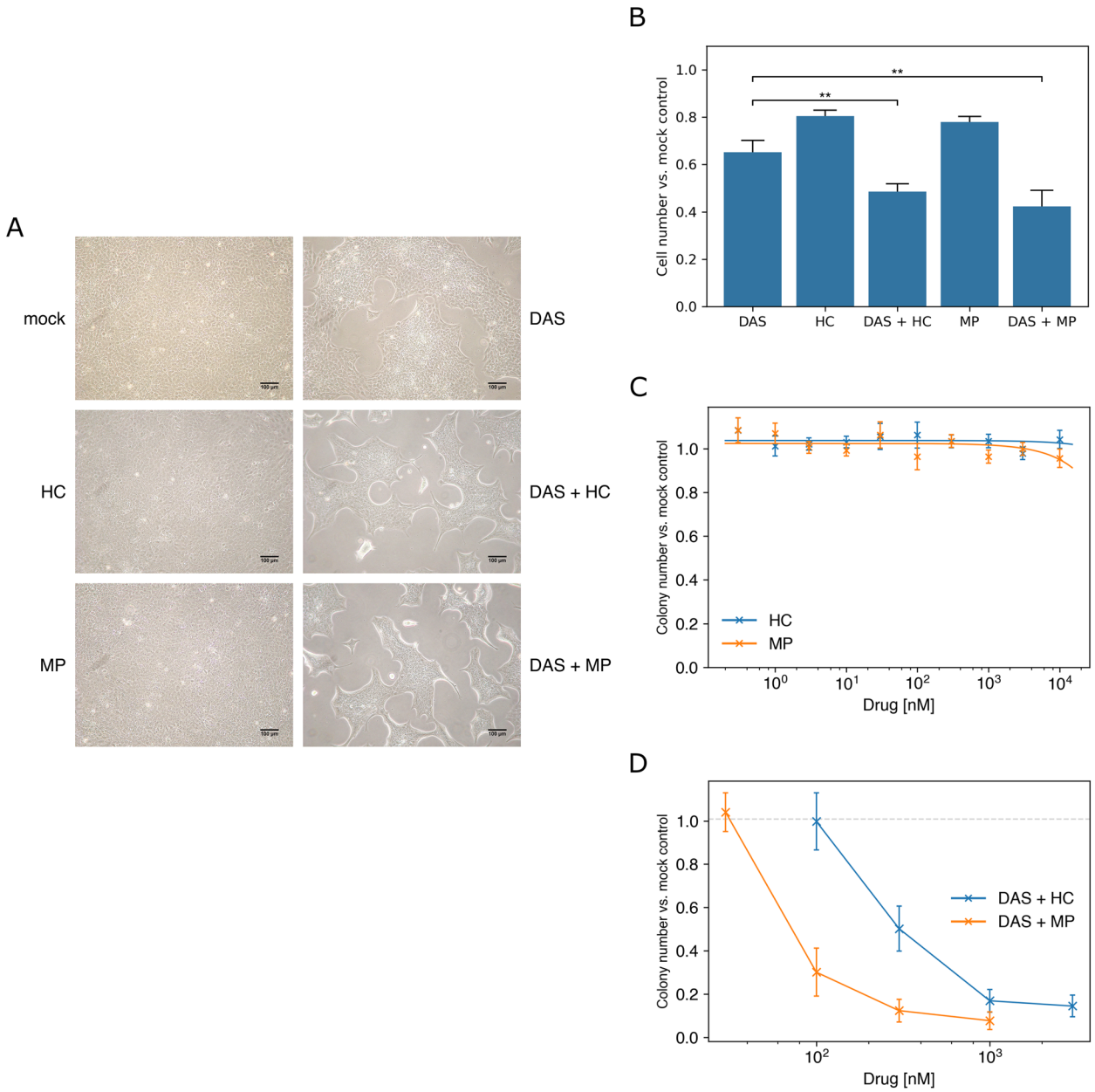

Fig. 6 Hydrocortisone and Methylprednisolone show synergistic activity with Dasatinib. **A** SAS cells were treated with DMSO (mock), 50 nM of DAS, 300 nM of HC, 150 nM of MP, a combination of DAS + HC or a combination of DAS + MP for 72 h. Bright-field images of SAS cell growth in 2D monolayer culture after 72 h of treatment. Images of SAS cells were captured with an inverted microscope using 10 × magnifications. **B** SAS cells were treated with DMSO (mock), 50 nM of DAS, 300 nM of HC, 150 nM of MP, a combination of DAS + HC or a combination of DAS + MP for 72 h. Viable SAS cell counts against mock control were evaluated by staining cells with trypan blue and counting of viable cells with an automated cell counter. Values are expressed as means and standard deviation obtained from three independent experiments. Asterisks indicate statistical significance for T-tests with p-values less than 0.01 (**).**C** HC and MP as single treatments show no reduction in the 3D soft agar colony formation of SAS cells as determined by colony counting. Data represent colony numbers normalized to mock-treated cells and show mean values ± SD of three independent experiments. **D** Concentration-dependent colony formation reduction of SAS cells in response to a fixed concentration of DAS (1 µM) and increasing concentrations of HC or MP in 3D soft agar culture. Data again represent colony numbers normalized to mock-treated cells and show mean values ± SD of three independent experiments

MP are pharmacologically achievable in human patient plasma upon normal dose administration [67, 68].

Discussion and conclusions

Molecularly targeted therapies are so far benefiting only a limited number of cancer patients. This is in part resulting from the high cost of these medicines [69], but also due to a limited arsenal of available drugs and our inability to reliably identify some of the patients who would significantly benefit from a particular type of targeted therapy [70]. The enormous heterogeneity of cancers on the molecular and biological level is at present only marginally understood. Even cancers arising in the same organ or body part can display an astounding degree of diversity. This has not yet been taken into sufficient consideration in the context of HNCs. Numerous preclinical and clinical studies have analyzed cancers originating from distinct sites of the head and neck as a more or less single entity rather than focusing on a specific tumor site [71]. However, epidemiological evidence and numerous studies by pathologists clearly show that major biological differences and clinical characteristics do exist between the different head and neck cancer sites and even sub-sites, as well as between different populations and individual patients with distinct underlying molecular defects [6, 72, 73]. Although there are now several targeted therapies for patients with HNSCC in clinical use [74], no particular targeted therapy for TSCC is available until now. More effective and more benign TSCC therapies are urgently needed. Identifying predictive tumor markers and new treatment targets, starting with cellular tumor models, is considered a valuable approach to achieving this.

Tyrosine kinases are frequent drivers of human tumor development but remain marginally studied in TSCC. Their mutation or hyper-activation often leads to constitutively elevated pTyr-protein levels that promote tumor progression. Our current preclinical approach, to find tyrosine kinases that are functionally implicated in the survival and growth of many different TSCC lines and to combine kinase inhibitor treatment by re-purposing other readily approved drugs, is hoped to be a rapid and cost-effective way forward in the quest for much better tumor treatments. Our starting point, a large panel of no less than 34 TSCC lines, was chosen in order to ensure that we focus on molecular targets shared by most, if not all, TSCC. Surprisingly, we found a high degree of similarity in the pTyr-protein patterns of our TSCC panel (Fig. 1A and Figure S1). A broad 130 kDa pTyr-protein band immediately reminded us of p130Cas [21], the major substrate of the Src kinase, which was discovered as the first oncogene more than 100 years ago in the form of a tumor virus [75]. Strikingly, inhibition of SFKs had a massive impact on overall pTyr-protein levels as well as p130Cas phosphorylation, thereby documenting that SFKs are major drivers of tyrosine phosphorylation in TSCC lines. Alterations of p130Cas expression and interactions and the resulting regulatory signals are determinants for the occurrence of different types of human tumors [76, 77].

In the past years, several observations suggested that aberrant activation of the p130Cas signaling network signature leads to up-regulation of key regulatory signaling pathways promoting cell transformation. For example, p130Cas silencing in HER2-dependent breast carcinoma reduces HER2 levels and impairs migration and invasion in vitro, as well as the formation of lung metastases in vivo [78–80]. Taken together, these results suggested to us that DAS could be a useful drug for TSCC therapy.

However, since targeted therapies are very frequently of time-limited use due the development of tumor resistances, and DAS may not be sufficiently effective when applied as monotherapy in head and neck cancer patients [13], we decided to screen for FDA-approved drugs that can be used in combination with DAS. One of the substance classes that emerged from this screen and became the central focus of the current work are glucocorticoids. They are in abundant and manifold clinical use, inexpensive and well-characterized. Interestingly, the inhibitory effects seen with DAS + GC combinations tended to be more striking in the soft agar assay, which monitors anchorage-independent (3D) growth, than in regular 2D cell culture. This implies that we may not have seen some possibly useful drug combination synergies in our high-throughput screen, carried out in classical 2D culture.

One of the most striking results from our experiments is the profound, albeit probably indirect, effect of even low GC concentrations on MET—Gab1 signaling in TSCC lines. Clinical MET inhibition in various cancers is highly desirable and therefore an area of intense research, but so far hampered by significant toxicity and, at least in some cases, a lack of sufficient efficacy, of clinically tested MET-targeting kinase inhibitors [81–83]. More specifically, MET signaling is also known to play a role in HNCs with respect to tumor development, therapeutic resistance and the behavior of the tumor microenvironment [84]. All three analyzed TSCC lines display a basal activity of MET—Gab1 signaling (Fig. 4A). This activity is sensitive even to subnanomolar concentrations of DX and FL (Fig. 4C). The exact mechanism behind this remains unclear, as DX does not directly inhibit MET kinase activity (Figure S5).

Some reports of glucocorticoid activity on the HGF—c-Met—Gab1 signaling pathway have been previously published, including a link between GC and Gab1 signaling related to asthma [85]. GCs have also been shown to

reduce HGF expression in cells for primary rat osteoblast cells [86]. This could potentially also occur in the TSCC lines, an avenue which remains to be explored.

Moreover, Gab1 has been shown to be important for the survival of HNSCC cells and a reduction of Gab1 expression led to impaired MAPK and PI3K—Akt signaling [87, 88]. This may, at least in part, be linked to the Gab1 effector phosphatase SHP2, since HNSCC cell lines were found to be particularly sensitive to the SHP2 inhibitor SHP099 when a large panel of over 800 cell lines of different tumor types was screened [88].

In any case, our current experiments have already provided several interesting leads into the pleiotropic functional biology of GCs in TSCC lines, which can now be followed up with more in-depth studies, in particular animal experiments. The full spectrum of bioactivity from DAS + GC treatments of TSCC lines will only become apparent once multiple signal transduction pathways and bioactivities are integrated and evaluated in vivo. The final functional outcomes of these integrative processes in the TSCC cell signaling networks are hard to predict. Consequently, the exact effects may vary from tumor to tumor, depending on the specific genetic and epigenetic alterations acquired during cancer development. Nevertheless, key results were found to be similar in three different cell lines, suggesting that they are likely to be representative for many other TSCC lines.

DAS, although clearly clinically useful and at present part of the standard anti-cancer drug portfolio in hospitals, may also be replaced in the future by more potent or more selective molecules, at least in some contexts. For example, the SFK inhibitor NXP900 [89], which is currently evaluated in early clinical trials, has shown striking activity in animal studies. NXP900 is reported to not only inhibit the kinase activity of SFK but also their kinase-independent scaffolding ability, increasing the potency of the inhibitor. Like DAS, its activity is enhanced when combined with other drugs. For example, NXP900 synergizes with the MEK inhibitor Trametinib in low grade serous ovarian cancer [90]. It is certainly worthwhile to test such newly arising, promising molecules in combination with different GCs for increased efficacy in TSCC in the near future. Moreover, the impact of GCs should be explored further in other squamous carcinomas of the head and neck region, in the hope of reducing the burden that our current HNC therapies elicit.

Methods

Reagents

PP2 (#529573) and PP3 (#529574) were purchased from Calbiochem, Dasatinib (#HY-10181) from Hycultec, and Crizotinib (#S1068) from Selleckchem. Dexamethasone (#D4902), Hydrocortisone (#H4001) and Methylprednisolone (#S1733) were obtained from Sigma-Aldrich. Antibodies against Src (#2108), pTyr416 Src (#2101), pTyr410 p130Cas (#4011), CDK1 (#9116), CDK2 (#2546), CDK4 (#12790), CDK6 (#13331), Cyclin B1 (#12231), WEE1 (#4936), pSer462 WEE1 (#4910), MET (#3148), pTyr1234/1235 MET (#3077), pTyr627 Gab1 (#3233) and pThr202/Tyr204 ERK 1/2 (#9101) were bought from Cell Signaling Technologies. Antibodies against p130CAS (#610271), Cyclin D3 (#610279) and p27Kip1 (#610241) were acquired from BD Biosciences. The antibody against Actin was purchased from Sigma-Aldrich (#A5441), anti-ERK 1/2 (#06–182) from Upstate Biotechnology and anti-Gab1 (#A303-288A) from Bethyl Laboratories. Secondary antibodies, HRP anti-mouse IgG (#715–036–151) and HRP anti-rabbit IgG (#711–036–152), were bought from Jackson ImmunoResearch Labs.

Cell lines and culture conditions

The origin of the 34 TSCC lines used in this study is described in Supplemental Table S1 and the literature [20]. All cell lines were initially established from primary tumors, except for the HSC-3, HSC-4, OSC-19 and OSC-20 cell lines, which were established from metastatic sites. Cells were cultured in Dulbecco's Modified Eagle Medium with high glucose and glutamine (DMEM, Gibco, #41966–029) supplemented with 10% heat-inactivated fetal bovine serum (FBS, Biowest, #S1860-500), 1% non-essential amino acids (NEAA, Gibco, #11140–035), and 1% penicillin/streptomycin (Gibco, #15140–122) at 37 °C in a humidified atmosphere with 10% CO_2. Cells were grown to 85–90% confluency and then passaged by trypsinization to avoid overgrowth.

Western blot analyses

TSCC cells were plated in 10-cm culture dishes and treated with the indicated compounds and concentrations. At the end of the treatments, proteins were extracted with RIPA lysis buffer (20 mM Tris–HCl pH 7.5, 1 mM EDTA, 100 mM NaCl, 1% (v/v) Triton X-100, 0.5% (w/v) DOC and 0.1% (w/v) SDS) in the presence of protease (1:40 cOmplete™ Protease Inhibitor Cocktail (Roche, #11836145001)) and phosphatase inhibitors (1:100 Phosphatase inhibitor cocktail 2 (Sigma Aldrich, #P5726), 1:100 Phosphatase inhibitor cocktail 3 (Sigma Aldrich, #P0044)). Protein concentrations were determined according to the method of Bradford. Equal amounts of proteins were separated by SDS-PAGE and transferred to a PVDF membrane by semi-dry transfer blotting. The membrane was then incubated for 1 h at room temperature (RT) in a blocking buffer (5% of BSA or milk in TBST (20 mM TrisHCl pH 7.5 and 100 mM NaCl with 0.1% (v/v) Tween 20)) as appropriate for

the individual antibody. It was then incubated with the respective primary antibody in blocking buffer overnight at 4 °C on a nutator. After washing three times with TBST, the membrane was incubated with horseradish peroxidase (HRP)-coupled secondary antibody for 1 h at RT. After washing three more times with TBST, a freshly mixed enhanced chemiluminescence (ECL) detection solution (Advansta, #K-12043-D10) was applied. The protein signals were detected on a chemiluminescence imaging system (Syngene G:BOX, Avantor).

MET kinase assays

SAS cells were seeded in 10 cm cell culture dishes, grown for 24 h and lysed with kinase lysis buffer (50 mM TrisHCl pH 7.5, 150 mM NaCl, 1% (v/v) Triton X-100, 1 mM EGTA, 1 mM EDTA and 1% (v/v) Glycerol) containing the appropriate inhibitors (0.5 ng/ml Leupeptin, 10 ng/ml Aprotinin, 200 ng/ml PMSF (DMSO), 1 mM Sodium orthovanadate, 1:100 Phosphatase inhibitor cocktail 2, 1:100 Phosphatase inhibitor cocktail 3 and 1:40 cOmplete™ Protease Inhibitor Cocktail). The cell lysate was agitated at 4 °C for 1 h, centrifuged and the supernatant was transferred to a new tube. The protein concentration was determined by Bradford assay. For pre-clearing, 10 µl amounts of G Sepharose beads (Cytiva, #17061801) were transferred into 1.5 ml tubes, washed twice with 500 µl of lysis buffer and mixed with 500 µg of protein cell lysate on a nutator at 4 °C for 1 h. Samples were centrifuged, the beads were discarded and the pre-cleared supernatants were transferred into new tubes. Subsequently, three types of immunoprecipitations were prepared (Table 1). 5 µg of mouse isotype control (Cell Signaling Technology, #5415) or 5 µg of MET antibody (Cell Signaling Technology, #8198) were added into the tubes containing pre-cleared lysates. Samples were agitated for 2 h at 4 °C, 10 µl G Sepharose beads were added and then mixed for 1 h at 4 °C. Then, the samples were centrifuged and the supernatants were discarded. The immunocomplexes were 3 × washed with 500 µl of washing buffer (20 mM TrisHCl pH 7.5, 100 mM NaCl, 1% (v/v) Triton X-100, 1 mM EGTA, 1 mM EDTA and 2.5% (v/v) glycerol) and kept on ice.

Samples were prepared as described in Table 2, added onto the immunocomplexes and incubated in a thermomixer (22 °C, 500 rpm) for 5 min. 5 µl of 20 mM ATP (pH 7.0) was added to all of the samples (except for the 'No ATP' control) to start the kinase reaction. Samples were again incubated in a thermomixer (22 °C, 500 rpm) for 30 min and the kinase reaction was stopped by addition of 50 µl SDS-PAGE sample buffers. Samples were immediately boiled at 95 °C for 15 min and centrifuged. 7.5 µg of the total cell lysate and 30 µl of the supernatants were separated by SDS-PAGE and analyzed by Western

Table 1 Types of samples generated for immunoprecipitation (IP)

Sample	Isotype control	No lysate control	Immunoprecipitation (IP)
Lysis buffer	X	same volume as lysate	X
Lysate	500 µg	X	500 µg
Antibody	5 µg isotype control	5 µg MET antibody	5 µg MET antibody

Table 2 Sample preparation for the MET kinase assay

Sample	Isotype control	No lysate control	No substrate control	No ATP control	Mock	Drug*
UC water (µl)	80	80	85	80	80 - drug volume	80 - drug volume
10x kinase buffer (µl)	10	10	10	10	10	10
Substrate (µl)**	5	5	X	5	5	5
DMSO (µl)	X	X	X	X	drug volume	X
Drug (µl)	X	X	X	X	X	drug volume
IP type (from table above)	Isotype control	No lysate control	IP	IP	IP	IP

*Dilutions of DX, Crizotinib and DMSO were prepared in washing buffer

**A recombinantly expressed His-tagged Gab1 (613-694) fusion protein was used as a kinase substrate. A pET42-based plasmid encoding for a His-tag and amino acids 613-694 of the human Gab1 protein, containing two tyrosine residues known to be phosphorylated in response to upstream receptor activation (Tyr627 and Tyr659), was expressed in *E.coli* BL21(DE3). The bacterial pellet was lysed by sonication in a buffer containing 20 mM sodium phosphate pH 7.3, 500 mM NaCl and protease inhibitors. Lysates were, after removal of bacterial debris by centrifugation, loaded onto a HiTrap IMAC FF column (Cytiva, Little Chalfont, UK) charged with Co^{2+}-ions. The His-tagged protein was eluted with a 15 mM to 500 mM imidazole gradient over 10 column volumes. The peak fractions were applied onto a HiLoad S75 pg column (Cytiva, Little Chalfont, UK) equilibrated with 50 mM sodium phosphate pH 7.3, 50 mM NaCl and finally concentrated in Vivaspin concentrator tubes with a molecular weight cut-off of 3000 Da (Sartorius, #VS2091)

blotting as described above with pTyr627 Gab1, total MET and pTyr1234/1235 MET antibodies.

Resazurin cell viability assays

The cytotoxicity of all compounds in 2D culture was evaluated by a resazurin assay. TSCC cells were washed with PBS, trypsinized, counted and seeded into 96-well plates at the appropriate cell densities to prevent confluence of the cells during the period of the experiment. For SAS, CAL27, and BICR56 cell lines 8000, 5000, and 3500 cells/well were seeded, respectively. After 24 h, the cells were treated with the investigated compounds or DMSO as vehicle control (mock). After treatment, the medium was discarded and each well was washed with 100 µl of PBS. The wells were then stained with 100 µl of 0.1% (w/v) resazurin (Sigma Aldrich, #199303) in DMEM without phenol red (Gibco, #21063–030) for about 2 h at 37 °C. The fluorescence at 590 nm was measured after excitation at 531 nm using a Infinite M Plex plate reader (Tecan, Männedorf, Switzerland). The percentages of surviving cells related to mock-treated cells were determined. Each experiment was repeated at least 3 times. Results are presented with the mean ± standard deviation.

Trypan blue exclusion assays

The Trypan Blue dye exclusion assay was used to determine the number of viable and dead cells in a cell suspension. For this, cells were plated in 6-well plates at the suitable cell numbers per well. For SAS, CAL27, and BICR56 cell lines, 240,000, 150,000, and 100,000 cells/well were seeded, respectively. On the following day, cells were exposed to different concentrations of agents or DMSO as vehicle control (mock). After 72 h of drug exposure, 10 µl of cell suspension was mixed with 10 µl of Trypan Blue (Invitrogen, #T10282) and pipetted into a disposable Countess cell counter chamber slide (Invitrogen, Waltham, MA, USA). Cell numbers were determined with an automated Countess II FL cell counter (Invitrogen, Waltham, MA, USA). Cell viability was calculated using the ratio of total live cells normalized to total live cells in the mock-treated sample. Each experiment was replicated three times.

Morphological evaluation by phase-contrast inverted microscope

Microscopic investigation was performed to identify the morphological features of treated cancer cells in comparison to mock-treated controls. For this, cells were seeded in 6-well plates and then treated with different concentrations of the investigated compounds or DMSO as vehicle control (mock). After 72 h of drug exposure, cell growth was evaluated with an inverted microscope (Eclipse TS100, Nikon) and photos were captured with a digital camera (Coolpix E5400, Nikon) at 10× and 20× magnifications.

3D soft agar assays

The anchorage-independent colony formation assay (soft agar assay) was performed as described previously [91]. 0.6% (w/v) Noble agar (BD Biosciences, #214,220) in 1×DMEM was plated as a bottom layer into 48-well plates placed on a pre-warmed glass plate (42 °C). Only the inner 24 wells of the 48-well plates were used, to avoid edge effect. Plates were left to harden for at least 30 min at RT in the cell culture hood. During that time, cells were trypsinized, diluted with 1×DMEM and counted. The cells were diluted with DMEM and mixed into 0.6% agar for a final agar concentration of 0.4% (6000 cells per well). This second layer was plated on top of the bottom (0.6% agar) layer. The plates were left again for at least 30 min at RT to solidify.

After solidification, 200 µl of DMEM with DMSO or compounds was added into each well. The cells were cultured at 37 °C in 10% CO_2 and the wells were fed every 3 to 4 days with 70 µl of DMEM with DMSO or compounds, stored since day 1, to prevent desiccation. After 14 days of incubation, cells were stained overnight at 37 °C by adding 70 µl of 0.5% nitroblue tetrazolium chloride (Roth, #4421.3) solution per well. Once colonies were stained, photographs of wells were taken using a Sony Alpha 5100 camera with a SEL30M35 macro lens. The colonies were counted using image analysis software (ImageJ 1.50i) using a minimum diameter of 50 µm as a cut-off for viable colonies. All experiments were conducted in triplicates. Calculation of IC_{50} values was performed in R 4.2.3. Values are presented as the means ± SEM from three independent experiments.

Cell cycle analyses

TSCC cells were seeded in 6-well plates for 24 h and treated with the indicated concentrations of each compound or DMSO as vehicle control (mock) for 72 h. The supernatant with the floating dead cells and the attached cells from each well were collected and fixed in 3 ml of cold ethanol at −20 °C overnight. Cells were stained with DAPI (1:10,000 dilution of a 20 mg/ml DAPI (Sigma Aldrich, #D9542) stock and 1:5,000 of 10 mg/ml RNAse A in PBS) for 30 min at 37 °C in the dark and then washed with PBS. Cell fluorescence was measured with a MACSQuant Analyzer 10 (Miltenyi Biotec) flow cytometer. Histograms of cell numbers vs. blue fluorescence were recorded and the distribution of cells in different cell cycle phases was determined based on the mean fluorescence intensity values. A total of 10,000 events were analyzed using the FlowJo (version 10) software.

Analysis of autophagy by acridine orange staining

Autophagy was investigated by the staining of acidic vesicular organelles with Acridine Orange (AO). TSCC cells were trypsinized, counted, seeded in 6-well plates for 24 h and then treated with the indicated concentration of each compound or DMSO as vehicle control (mock) for 72 h. Cells were then collected, washed with PBS and stained with 500 µl of 10 µM AO solution (Sigma Aldrich, #235,474) for 15 min at 37 °C in the dark. Afterwards, cells were washed with PBS to remove excess AO and the cell pellet was resuspended in 500 µl PBS for flow cytometry analysis with the MACSQuant Analyzer 10 (Miltenyi Biotec) flow cytometer. A total of 10,000 events were analyzed using the FlowJo (version 10) software.

Senescence detection by β-Galactosidase staining

To detect the senescence state of the cells, treated TSCC were stained using a Senescence associated β-galactosidase (SA-β-gal) Staining Kit (Cell Signaling Technology, #9860) according to the manufacturer's instructions.

Briefly, TSCC cells were seeded in 6-well plates for 24 h and treated for 72 h with the investigated compounds or DMSO as vehicle control (mock). The growth medium was discarded, the cells were washed with PBS and fixed in 2% paraformaldehyde for 15 min at RT. After washing twice with PBS, they were incubated overnight with the β-Galactosidase staining solution at 37 °C in a dry incubator without additional CO_2. On the next day, while the β-Galactosidase was still on the plate, the cells were analyzed under the Eclipse microscope for the development of blue color and photographed with a digital camera (Coolpix E5400, Nikon).

Life cell imaging

SAS cells were seeded at 150,000 cells per well into 24-well plates and left to attach for 24 h. The medium was then replaced with fresh medium containing 0.05% DMSO or 30 µM PP2. The plates were transferred into the Cell-IQ imaging system (Chip-Man Technologies Ltd). Photographs were taken at the same location every 20 min over 5 days. The Cell-IQ ImgenTM Software Package and Cell-IQ Analyser® software package were used to analyze the images and to create movie files.

High-throughput screening and analysis

Three cell lines (BICR56, CAL27, and SAS) were used for high-throughput screening. Their identity was confirmed by STR profiling (Microsynth AG, Balgach, Switzerland) and the cells were free of mycoplasma as determined by PCR testing [92]. The cells were treated with a combination of DAS (0 µM or 0.03 µM) and FDA-approved drugs from the Pharmakon 1600 library (MicroSource Discovery Systems, Inc.; Gaylordsville, CT, USA) at three concentrations (0.4 µM, 2 µM, 10 µM). There was one biological replicate per treatment.

The compound library consisted of 20 library plates with 80 compounds each. The treatment was performed on seven different days as a maximum of three library plates could be processed within one day.

In preparation for each treatment day, cells were thawed from a frozen stock and passaged twice. The cells were then trypsinized, seeded into 96-well plates at 2700 (SAS), 4700 (CAL27) or 3400 (BICR56) cells/ well using a Flexdrop Plus dispenser (PerkinElmer, Waltham (MA), USA) and grown for one more day at 37 °C and 10% CO_2. Compounds and controls were applied onto 96-well plates in a Janus MDT workstation (PerkinElmer, Waltham (MA), USA). On all plates, four wells each were reserved for medium-only, Staurosporine, DMSO, and DAS-only controls. All plates were prepared in duplicate.

The medium was replaced after three days on the Janus MDT workstation against DMEM without phenol red but containing resazurin (100 µg/ml). After another 2 h incubation, the metabolic activity was assessed by fluorescence measurement (excitation 531 nm, emission 595 nm) on an Envision Multilabel Reader (PerkinElmer, Waltham, MA, USA). r^2 values (linear regression) were determined for plate duplicates. Plates with an r^2 of less than 0.7 were excluded from further analysis (26 of 720 plates). Ratios for the two replicate wells, on different plates, were calculated. Outliers (1.5 × interquartile range) were excluded from further analysis (45 of 34,560 pairs). All sample wells on each plate were then normalized with the mean of their four DMSO-control wells. The mean of the two replicate sample wells from these DMSO-normalized plates was used for further analysis.

Ratios of cells treated with a combination of compound and DAS against the compound alone were $\log_2$-transformed for an approximately normal distribution and analyzed for outliers (1.5 × interquartile range). Drugs that showed potential synergy in more than one cell line were considered to be the most promising candidates for further analyses.

Statistical analyses

Data are presented as mean ± standard deviation, unless indicated otherwise. Model fits for EC_{50} estimation and standard error calculation were performed in R 4.2.3 [93] using the 'drc' 3.0–1 package 'LL.4' four-parameter log-logistic function [94]. T-tests were calculated with pingouin 0.5.4 [95]. Further statistical analysis was done with pandas 2.0.3 [96] and numpy 1.24.3 [97]. Charts were generated in Python 3.11.5 using the matplotlib 3.7.2 [98] and Seaborn 0.12.2 [99] libraries.

Abbreviations

AO	Acridin Orange
DAS	Dasatinib
CML	Chronic myelogenous leukemia
DX	Dexamethasone
EMT	Epithelial-mesenchymal transition
FL	Fluticasone
GC	Glucocorticoid
HC	Hydrocortisone
HNC	Head and neck cancer
HNSCC	Head and neck squamous cell carcinoma
HPV	Human papilloma virus
MAPK	Mitogen-activated protein kinase
MP	Methylprednisolone
OSCC	Oral squamous cell carcinoma
PTK	Protein tyrosine kinase
RTK	Receptor tyrosine kinase
SA-β-gal	Senescence-associated beta-galactosidase
SFK	Src family kinases
TSCC	Tongue squamous cell carcinoma

Supplementary Information

The online version contains supplementary material available at https://doi.org/10.1186/s12964-025-02129-8.

Supplementary Material 1. Data S1. High-throughput screen results.

Supplementary Material 2. Table S1. Cell line information.

Supplementary Material 3. Video S1. Live cell imaging of SAS cells treated with PP2.

Supplementary Material 4. Supplementary figures and legends.

Acknowledgements
We would like to thank Elena Seraia, formerly at the Target Discovery Institute, Oxford, UK, for supervising the practical part of the HTP screen and many interesting stories about life in Novosibirsk. We would also like to thank Nadine Bley, Core Facility Imaging (Martin-Luther-University Halle-Wittenberg, Germany), for her help in performing the flow cytometry experiments and the data analysis.

Authors' contributions
AH performed the major part of the biochemical experiments and analyses. JD investigated the patterns of phosphotyrosine proteins in the TSCC panel and performed experiments with SFK inhibitors. DE designed the HTP screen. SF conceived the project and supervised the work. ML performed the HTP screen, analyzed the data and supervised the work. AH, SF and ML drafted the manuscript. JD and DE commented on and approved the manuscript.

Funding
We are greatly indebted to the charity HeadsUp, Oxford, UK (now joined with Oracle Cancer Trust) and to the Wilhelm-Sander-Stiftung Munich, Germany (grants 2015.102.1 and 2015.102.2 to SF), for funding parts of this work. A.H. gratefully acknowledges financial support from Yarmouk University, Irbid, Jordan, during his scientific research visit at the Martin-Luther-University Halle-Wittenberg.

Data availability
The dataset that was generated and analysed during this study is included in the supplementary materials (Data S1).

Declarations

Competing interests
The authors declare no competing interests.

Author details
[1]Institute of Molecular Medicine, Medical Faculty of the Martin-Luther-University Halle-Wittenberg, Halle (Saale), Germany. [2]Department of Pharmaceutics and Pharmaceutical Technology, Faculty of Pharmacy, Yarmouk University, Irbid, Jordan. [3]Nuffield Department of Surgical Sciences, Medical Sciences Division, University of Oxford, Oxford, UK. [4]Nuffield Department of Medicine, University of Oxford, Oxford, UK.

Received: 22 October 2024 Accepted: 25 February 2025
Published online: 19 June 2025

References

1. Tan Y, Wang Z, Xu M, Li B, Huang Z, Qin S, et al. Oral squamous cell carcinomas: state of the field and emerging directions. Int J Oral Sci. 2023;15:44.
2. Zhu L, Wang Y, Li R, Liu A, Zhang X, Zuo C, et al. Surgical treatment of early tongue squamous cell carcinoma and patient survival. Oncol Lett. 2019;17:5681–5.
3. Nemade H, Chaitanya SA, Kumar S, A AK, Rao TS, Rao SLMCS. Oncological outcomes of total glossectomy procedure for advanced tongue cancer: a single-centre experience. Int J Oral Maxillofac Surg. 2022;51:152–8.
4. Katna R, Bhosale B, Sharma R, Singh S, Deshpande A, Kalyani N. Oncological outcomes in patients undergoing major glossectomy for advanced carcinoma of the oral tongue. Ann R Coll Surg Engl. 2020;102:514–8.
5. Vettore AL, Ramnarayanan K, Poore G, Lim K, Ong CK, Huang KK, et al. Mutational landscapes of tongue carcinoma reveal recurrent mutations in genes of therapeutic and prognostic relevance. Genome Med. 2015;7:98.
6. Leemans CR, Snijders PJF, Brakenhoff RH. The molecular landscape of head and neck cancer. Nat Rev Cancer. 2018;18:269–82.
7. Li Q, Tie Y, Alu A, Ma X, Shi H. Targeted therapy for head and neck cancer: signaling pathways and clinical studies. Signal Transduct Target Ther. 2023;8:31.
8. Zhou Y, Yao Z, Lin Y, Zhang H. From Tyrosine kinases to tyrosine phosphatases: new therapeutic targets in cancers and beyond. Pharmaceutics. 2024;16: 888.
9. Bou Antoun N, Chioni A-M. Dysregulated signalling pathways driving anticancer drug resistance. Int J Mol Sci. 2023;24: 12222.
10. Kim LC, Song L, Haura EB. Src kinases as therapeutic targets for cancer. Nat Rev Clin Oncol. 2009;6:587–95.
11. Hanke JH, Gardner JP, Dow RL, Changelian PS, Brissette WH, Weringer EJ, et al. Discovery of a novel, potent, and Src family-selective tyrosine kinase inhibitor. Study of Lck- and FynT-dependent T cell activation. J Biol Chem. 1996;271:695–701.
12. Olivieri A, Manzione L. Dasatinib: a new step in molecular target therapy. Ann Oncol. 2007;18 Suppl 6:vi42–46.
13. Brooks HD, Glisson BS, Bekele BN, Johnson FM, Ginsberg LE, El-Naggar A, et al. Phase 2 study of dasatinib in the treatment of head and neck squamous cell carcinoma. Cancer. 2011;117:2112–9.
14. Fury MG, Baxi S, Shen R, Kelly KW, Lipson BL, Carlson D, et al. Phase II study of saracatinib (AZD0530) for patients with recurrent or metastatic head and neck squamous cell carcinoma (HNSCC). Anticancer Res. 2011;31:249–53.
15. Hermida-Prado F, Villaronga MÁ, Granda-Díaz R, Del-Río-Ibisate N, Santos L, Hermosilla MA, et al. The SRC inhibitor dasatinib induces stem cell-like properties in head and neck cancer cells that are effectively counteracted by the mithralog EC-8042. J Clin Med. 2019;8: 1157.
16. Pufall MA. Glucocorticoids and Cancer. Adv Exp Med Biol. 2015;872:315–33.
17. Kim KN, LaRiviere M, Macduffie E, White CA, Jordan-Luft MM, Anderson E, et al. Use of glucocorticoids in patients with cancer: potential benefits, harms, and practical considerations for clinical practice. Pr Radiat Oncol. 2023;13:28–40.
18. Sachs M, Brohmann H, Zechner D, Müller T, Hülsken J, Walther I, et al. Essential role of Gab1 for signaling by the c-Met receptor in vivo. J Cell Biol. 2000;150:1375–84.

19. Itoh M, Yoshida Y, Nishida K, Narimatsu M, Hibi M, Hirano T. Role of Gab1 in heart, placenta, and skin development and growth factor- and cytokine-induced extracellular signal-regulated kinase mitogen-activated protein kinase activation. Mol Cell Biol. 2000;20:3695–704.
20. Wu Z, Doondeea JB, Gholami AM, Janning MC, Lemeer S, Kramer K, et al. Quantitative chemical proteomics reveals new potential drug targets in head and neck cancer. Mol Cell Proteomics. 2011;10:M111 .011635.
21. Emaduddin M, Bicknell DC, Bodmer WF, Feller SM. Cell growth, global phosphotyrosine elevation, and c-Met phosphorylation through Src family kinases in colorectal cancer cells. Proc Natl Acad Sci U A. 2008;105:2358–62.
22. Sakai R, Iwamatsu A, Hirano N, Ogawa S, Tanaka T, Mano H, et al. A novel signaling molecule, p130, forms stable complexes in vivo with v-Crk and v-Src in a tyrosine phosphorylation-dependent manner. EMBO J. 1994;13:3748–56.
23. Lewitzky M, Simister PC, Feller SM. Beyond "furballs" and "dumpling soups" - towards a molecular architecture of signaling complexes and networks. FEBS Lett. 2012;586:2740–50.
24. Camacho Leal MDP, Sciortino M, Tornillo G, Colombo S, Defilippi P, Cabodi S. p130Cas/BCAR1 scaffold protein in tissue homeostasis and pathogenesis. Gene. 2015;562:1–7.
25. Tikhmyanova N, Little JL, Golemis EA. CAS proteins in normal and pathological cell growth control. Cell Mol Life Sci. 2010;67:1025–48.
26. Barrett A, Pellet-Many C, Zachary IC, Evans IM, Frankel P. p130Cas: a key signalling node in health and disease. Cell Signal. 2013;25:766–77.
27. Defilippi P, Di Stefano P, Cabodi S. p130Cas: a versatile scaffold in signaling networks. Trends Cell Biol. 2006;16:257–63.
28. Kumbrink J, Soni S, Laumbacher B, Loesch B, Kirsch KH. Identification of Novel Crk-associated Substrate (p130Cas) Variants with Functionally Distinct Focal Adhesion Kinase Binding Activities. J Biol Chem. 2015;290:12247–55.
29. Liu D, Peterson ME, Long EO. The adaptor protein Crk controls activation and inhibition of natural killer cells. Immunity. 2012;36:600–11.
30. Mitra SK, Schlaepfer DD. Integrin-regulated FAK-Src signaling in normal and cancer cells. Curr Opin Cell Biol. 2006;18:516–23.
31. Bain J, Plater L, Elliott M, Shpiro N, Hastie CJ, McLauchlan H, et al. The selectivity of protein kinase inhibitors: a further update. Biochem J. 2007;408:297–315.
32. Brandvold KR, Santos SM, Breen ME, Lachacz EJ, Steffey ME, Soellner MB. Exquisitely specific bisubstrate inhibitors of c-Src kinase. ACS Chem Biol. 2015;10:1387–91.
33. Lee S, Park S, Ryu J-S, Kang J, Kim I, Son S, et al. c-Src inhibitor PP2 inhibits head and neck cancer progression through regulation of the epithelial-mesenchymal transition. Exp Biol Med Maywood. 2023;248:492–500.
34. Piwnica-Worms H, Saunders KB, Roberts TM, Smith AE, Cheng SH. Tyrosine phosphorylation regulates the biochemical and biological properties of pp60c-src. Cell. 1987;49:75–82.
35. Lindauer M, Hochhaus A. Dasatinib. Recent Results Cancer Res. 2018;212:29–68.
36. Demetri GD, Lo Russo P, MacPherson IRJ, Wang D, Morgan JA, Brunton VG, et al. Phase I dose-escalation and pharmacokinetic study of dasatinib in patients with advanced solid tumors. Clin Cancer Res. 2009;15:6232–40.
37. Mayer BJ, Hirai H, Sakai R. Evidence that SH2 domains promote processive phosphorylation by protein-tyrosine kinases. Curr Biol. 1995;5:296–305.
38. Sakai R, Nakamoto T, Ozawa K, Aizawa S, Hirai H. Characterization of the kinase activity essential for tyrosine phosphorylation of p130Cas in fibroblasts. Oncogene. 1997;14:1419–26.
39. Manley PW, Cowan-Jacob SW, Buchdunger E, Fabbro D, Fendrich G, Furet P, et al. Imatinib: a selective tyrosine kinase inhibitor. Eur J Cancer. 2002;38 Suppl 5:S19–27.
40. Li H, Wawrose JS, Gooding WE, Garraway LA, Lui VWY, Peyser ND, et al. Genomic analysis of head and neck squamous cell carcinoma cell lines and human tumors: a rational approach to preclinical model selection. Mol Cancer Res MCR. 2014;12:571–82.
41. Prime SS, Eveson JW, Stone AM, Huntley SP, Davies M, Paterson IC, et al. Metastatic dissemination of human malignant oral keratinocyte cell lines following orthotopic transplantation reflects response to TGF-beta 1. J Pathol. 2004;203:927–32.
42. Jiang L, Ji N, Zhou Y, Li J, Liu X, Wang Z, et al. CAL 27 is an oral adenosquamous carcinoma cell line. Oral Oncol. 2009;45:e204–207.
43. Chen C-Y, Chiou S-H, Huang C-Y, Jan C-I, Lin S-C, Tsai M-L, et al. Distinct population of highly malignant cells in a head and neck squamous cell carcinoma cell line established by xenograft model. J Biomed Sci. 2009;16: 100.
44. Palmer AC, Sorger PK. Combination Cancer Therapy Can Confer Benefit via Patient-to-Patient Variability without Drug Additivity or Synergy. Cell. 2017;171:1678–1691.e13.
45. Silva JPN, Pinto B, Monteiro L, Silva PMA, Bousbaa H. Combination Therapy as a Promising Way to Fight Oral Cancer. Pharmaceutics. 2023;15: 1653.
46. Mackie AE, Ventresca GP, Fuller RW, Bye A. Pharmacokinetics of intravenous fluticasone propionate in healthy subjects. Br J Clin Pharmacol. 1996;41:539–42.
47. Vargas R, Dockhorn RJ, Findlay SR, Korenblat PE, Field EA, Kral KM. Effect of fluticasone propionate aqueous nasal spray versus oral prednisone on the hypothalamic-pituitary-adrenal axis. J Allergy Clin Immunol. 1998;102:191–7.
48. Madamsetty VS, Mohammadinejad R, Uzieliene I, Nabavi N, Dehshahri A, García-Couce J, et al. Dexamethasone: Insights into Pharmacological Aspects, Therapeutic Mechanisms, and Delivery Systems. ACS Biomater Sci Eng. 2022;8:1763–90.
49. Oakley RH, Cidlowski JA. The biology of the glucocorticoid receptor: new signaling mechanisms in health and disease. J Allergy Clin Immunol. 2013;132:1033–44.
50. Rothenberger NJ, Stabile LP. Hepatocyte Growth Factor/c-Met Signaling in Head and Neck Cancer and Implications for Treatment. Cancers Basel. 2017;9:39.
51. Giordano S, Di Renzo MF, Narsimhan RP, Cooper CS, Rosa C, Comoglio PM. Biosynthesis of the protein encoded by the c-met proto-oncogene. Oncogene. 1989;4:1383–8.
52. Den Haese GJ, Walworth N, Carr AM, Gould KL. The Wee1 protein kinase regulates T14 phosphorylation of fission yeast Cdc2. Mol Biol Cell. 1995;6:371–85.
53. Katayama K, Fujita N, Tsuruo T. Akt/protein kinase B-dependent phosphorylation and inactivation of WEE1Hu promote cell cycle progression at G2/M transition. Mol Cell Biol. 2005;25:5725–37.
54. Ge H, Ke J, Xu N, Li H, Gong J, Li X, et al. Dexamethasone alleviates pemetrexed-induced senescence in Non-Small-Cell Lung Cancer. Food Chem Toxicol. 2018;119:86–97.
55. Starling S. Glucocorticoid-induced bone loss linked with marrow adipocyte senescence. Nat Rev Endocrinol. 2023;19:312.
56. Patki M, McFall T, Rosati R, Huang Y, Malysa A, Polin L, et al. Chronic p27Kip1 Induction by Dexamethasone Causes Senescence Phenotype and Permanent Cell Cycle Blockade in Lung Adenocarcinoma Cells Over-expressing Glucocorticoid Receptor. Sci Rep. 2018;8:16006.
57. Ge H, Ni S, Wang X, Xu N, Liu Y, Wang X, et al. Dexamethasone reduces sensitivity to cisplatin by blunting p53-dependent cellular senescence in non-small cell lung cancer. PLoS ONE. 2012;7: e51821.
58. Srivastava S, Siddiqui S, Singh S, Chowdhury S, Upadhyay V, Sethi A, et al. Dexamethasone induces cancer mitigation and irreversible senescence in lung cancer cells via damaging cortical actin and sustained hyperphosphorylation of pRb. Steroids. 2023;198: 109269.
59. Kullmann MK, Grubbauer C, Goetsch K, Jäkel H, Podmirseg SR, Trockenbacher A, et al. The p27-Skp2 axis mediates glucocorticoid-induced cell cycle arrest in T-lymphoma cells. Cell Cycle. 2013;12:2625–35.
60. Levy JMM, Towers CG, Thorburn A. Targeting autophagy in cancer. Nat Rev Cancer. 2017;17:528–42.
61. Grandér D, Kharaziha P, Laane E, Pokrovskaja K, Panaretakis T. Autophagy as the main means of cytotoxicity by glucocorticoids in hematological malignancies. Autophagy. 2009;5:1198–200.
62. Liu L, Han S, Xiao X, An X, Gladkich J, Hinz U, et al. Glucocorticoid-induced microRNA-378 signaling mediates the progression of pancreatic cancer by enhancing autophagy. Cell Death Dis. 2022;13:1052.
63. Tan Y-Q, Zhang J, Zhou G. Autophagy and its implication in human oral diseases. Autophagy. 2017;13:225–36.
64. Xu J, Su Y, Xu A, Fan F, Mu S, Chen L, et al. miR-221/222-Mediated Inhibition of Autophagy Promotes Dexamethasone Resistance in Multiple Myeloma. Mol Ther. 2019;27:559–70.
65. Jiang L, Xu L, Xie J, Li S, Guan Y, Zhang Y, et al. Inhibition of autophagy overcomes glucocorticoid resistance in lymphoid malignant cells. Cancer Biol Ther. 2015;16:466–76.

66. SenthilKumar G, Skiba JH, Kimple RJ. High-throughput quantitative detection of basal autophagy and autophagic flux using image cytometry. Biotechniques. 2019;67:70–3.
67. Werumeus Buning J, Touw DJ, Brummelman P, Dullaart RPF, van den Berg G, van der Klauw MM, et al. Pharmacokinetics of oral hydrocortisone - Results and implications from a randomized controlled trial. Metabolism. 2017;71:7–16.
68. Jayne DRW, Gaskin G, Rasmussen N, Abramowicz D, Ferrario F, Guillevin L, et al. Randomized trial of plasma exchange or high-dosage methylprednisolone as adjunctive therapy for severe renal vasculitis. J Am Soc Nephrol. 2007;18:2180–8.
69. Leighl NB, Nirmalakumar S, Ezeife DA, Gyawali B. An Arm and a Leg: The Rising Cost of Cancer Drugs and Impact on Access. Am Soc Clin Oncol Educ Book. 2021;41:1–12.
70. Lee YT, Tan YJ, Oon CE. Molecular targeted therapy: Treating cancer with specificity. Eur J Pharmacol. 2018;834:188–96.
71. Vermorken JB, Mesia R, Rivera F, Remenar E, Kawecki A, Rottey S, et al. Platinum-based chemotherapy plus cetuximab in head and neck cancer. N Engl J Med. 2008;359:1116–27.
72. De Cecco L, Nicolau M, Giannoccaro M, Daidone MG, Bossi P, Locati L, et al. Head and neck cancer subtypes with biological and clinical relevance: Meta-analysis of gene-expression data. Oncotarget. 2015;6:9627–42.
73. Morris LGT, Chandramohan R, West L, Zehir A, Chakravarty D, Pfister DG, et al. The Molecular Landscape of Recurrent and Metastatic Head and Neck Cancers: Insights From a Precision Oncology Sequencing Platform. JAMA Oncol. 2017;3:244–55.
74. Kitamura N, Sento S, Yoshizawa Y, Sasabe E, Kudo Y, Yamamoto T. Current Trends and Future Prospects of Molecular Targeted Therapy in Head and Neck Squamous Cell Carcinoma. Int J Mol Sci. 2020;22: 240.
75. Weiss RA, Vogt PK. 100 years of Rous sarcoma virus. J Exp Med. 2011;208:2351–5.
76. Li J, Zhang X, Hou Z, Cai S, Guo Y, Sun L, et al. P130cas-FAK interaction is essential for YAP-mediated radioresistance of non-small cell lung cancer. Cell Death Dis. 2022;13:783.
77. Pincini A, Tornillo G, Orso F, Sciortino M, Bisaro B, Leal MDPC, et al. Identification of p130Cas/ErbB2-dependent invasive signatures in transformed mammary epithelial cells. Cell Cycle. 2013;12:2409–22.
78. Cabodi S, Tinnirello A, Di Stefano P, Bisarò B, Ambrosino E, Castellano I, et al. p130Cas as a new regulator of mammary epithelial cell proliferation, survival, and HER2-neu oncogene-dependent breast tumorigenesis. Cancer Res. 2006;66:4672–80.
79. Cabodi S, Tinnirello A, Bisaro B, Tornillo G, del Pilar C-L, Forni G, et al. p130Cas is an essential transducer element in ErbB2 transformation. FASEB J. 2010;24:3796–808.
80. Bisaro B, Sciortino M, Colombo S, Camacho Leal MP, Costamagna A, Castellano I, et al. p130Cas scaffold protein regulates ErbB2 stability by altering breast cancer cell sensitivity to autophagy. Oncotarget. 2016;7:4442–53.
81. Guo R, Luo J, Chang J, Rekhtman N, Arcila M, Drilon A. MET-dependent solid tumours - molecular diagnosis and targeted therapy. Nat Rev Clin Oncol. 2020;17:569–87.
82. Puccini A, Marín-Ramos NI, Bergamo F, Schirripa M, Lonardi S, Lenz H-J, et al. Safety and Tolerability of c-MET Inhibitors in Cancer. Drug Saf. 2019;42:211–33.
83. Choueiri TK, Halabi S, Sanford BL, Hahn O, Michaelson MD, Walsh MK, et al. Cabozantinib Versus Sunitinib As Initial Targeted Therapy for Patients With Metastatic Renal Cell Carcinoma of Poor or Intermediate Risk: The Alliance A031203 CABOSUN Trial. J Clin Oncol. 2017;35:591–7.
84. Hartmann S, Bhola NE, Grandis JR. HGF/Met Signaling in Head and Neck Cancer: Impact on the Tumor Microenvironment. Clin Cancer Res. 2016;22:4005–13.
85. Sharma A, Menche J, Huang CC, Ort T, Zhou X, Kitsak M, et al. A disease module in the interactome explains disease heterogeneity, drug response and captures novel pathways and genes in asthma. Hum Mol Genet. 2015;24:3005–20.
86. Blanquaert F, Pereira RC, Canalis E. Cortisol inhibits hepatocyte growth factor/scatter factor expression and induces c-met transcripts in osteoblasts. Am J Physiol Endocrinol Metab. 2000;278:E509–515.
87. Hoeben A, Martin D, Clement PM, Cools J, Gutkind JS. Role of GRB2-associated binder 1 in epidermal growth factor receptor-induced signaling in head and neck squamous cell carcinoma. Int J Cancer. 2013;132:1042–50.
88. Kurupi R, Floros KV, Jacob S, Chawla AT, Cai J, Hu B, et al. Pharmacologic Inhibition of SHP2 Blocks Both PI3K and MEK Signaling in Low-epiregulin HNSCC via GAB1. Cancer Res Commun. 2022;2:1061–74.
89. Dash S, Hanson S, King B, Nyswaner K, Foss K, Tesi N, et al. The SRC family kinase inhibitor NXP900 demonstrates potent antitumor activity in squamous cell carcinomas. J Biol Chem. 2024;300: 107615.
90. Hollis RL, Elliott R, Dawson JC, Ilenkovan N, Matthews RM, Stillie LJ, et al. High throughput screening identifies dasatinib as synergistic with trametinib in low grade serous ovarian carcinoma. Gynecol Oncol. 2024;186:42–52.
91. Borowicz S, Van Scoyk M, Avasarala S, Karuppusamy Rathinam MK, Tauler J, Bikkavilli RK, et al. The soft agar colony formation assay. J Vis Exp. 2014;92:e51998. https://doi.org/10.3791/51998.
92. Uphoff CC, Drexler HG. Comparative PCR analysis for detection of mycoplasma infections in continuous cell lines. Vitro Cell Dev Biol Anim. 2002;38:79–85.
93. R Core Team. R: a language and environment for statistical computing. Vienna: R Foundation for Statistical Computing; 2023. Available from: https://www.R-project.org/.
94. Ritz C, Baty F, Streibig JC, Gerhard D. Dose-response analysis using R. PLoS One 2015;10. Available from: http://journals.plos.org/plosone/article?id=10.1371/journal.pone.0146021.
95. Vallat R. Pingouin: statistics in Python. J Open Source Softw. 2018;3:1026.
96. team T pandas development. pandas-dev/pandas: Pandas. Zenodo. 2023. https://doi.org/10.5281/zenodo.8092754.
97. Harris CR, Millman KJ, van der Walt SJ, Gommers R, Virtanen P, Cournapeau D, et al. Array programming with NumPy. Nature. 2020;585:357–62.
98. Caswell TA, Andrade ES de, Lee A, Droettboom M, Hoffmann T, Klymak J, et al. matplotlib/matplotlib: REL: v3.7.2. Zenodo. 2023. https://doi.org/10.5281/zenodo.8118151.
99. Waskom ML. seaborn: statistical data visualization. J Open Source Softw. 2021;6:3021.

Publisher's Note